Advanced Steel Construction – Vol. 22 No. 3 (2026) 263–274
DOI:10.18057/IJASC.2026.22.3.2

MEASUREMENT POINT OPTIMIZATION METHOD FOR LARGE-SPAN SPACE STRUCTURES BASED ON STRUCTURAL RESPONSE CORRELATION

Ren-Zhang Yan [1, *], Wei Liu [1], Yang Liu [2], Chun-Ling Yan [1] and Tao Zhu [1]

[1] *School of Civil Engineering, Chongqing Jiaotong University, Chongqing 400074, China*
[2] *The 9th Engineering Co., Ltd. of CCCC First Highway Engineering Co., Ltd., Guangzhou 510000, China*
* *(Corresponding author: E-mail: rz_yan@cqjtu.edu.cn)*

ABSTRACT

The mechanical properties of large-span space structures are complicated and change greatly during its construction. So it is necessary to monitor the real time status of the structure to ensure the safety of the construction process. However, the number of monitoring points is often very large due to the space structure's large number of members and three-dimensional forcing characteristics. An optimization method for reducing monitoring points is proposed based on the characteristics of certain correlation between different members' mechanical responses during construction in this paper. Firstly, the comprehensive correlation matrix of structural response was established by using correlation coefficient method and grey correlation degree method, and the cluster correlation matrix with block characteristics was calculated by the bond energy algorithm, so as to construct the classification and optimization principle of reducing measuring points. Then, LSTM neural network was used to build a response prediction model, and the in-situ monitoring data was used to train and verify the prediction model. The results show that Pearson correlation coefficient and B-type grey correlation can effectively explore the similarity between the change size and trend of spatial structural responses. At the same time, LSTM neural network can learn to optimize the response correlation between the measuring points and its related measuring points, realizing the global monitoring of the structure.

ARTICLE HISTORY

Received: 20 February 2025
Revised: 4 August 2025
Accepted: 18 August 2025

KEYWORDS

Large-span space structure;
Response correlation;
Measurement point optimization;
Neural network

1. Introduction

Due to their large scale and the fact that large-span space structures usually undergo multiple structural system transformations during the construction process, the construction process often becomes the most dangerous stage in their entire life cycle. Therefore, in order to ensure the construction safety of large-span space structures, sensors need to be deployed on key members of the structure to obtain the real-time status of the structure. However, there are a lot of rods in large-span space structures, and they are in a three-dimensional spatial forcing state. There are also many measuring points, which greatly increases the cost and maintenance difficulty of the entire monitoring system. At the same time, more measurement points also increase the amount of data collection, which leads to a large number of data redundancy and increases the cost of later data analysis and storage. To this end, scholars at home and abroad have conducted a series of studies on the optimization of measurement points. For example, both Peng[1] and Lu[2] used the Pearson correlation coefficients to measure the correlation between the responses of the measurement points, established a correlation matrix of structural response, and achieved better arrangement of structural measuring points; Zhu[3] also adopted the Pearson correlation coefficient to calculate and analyze the correlation between multi-strain sensors, and establish a correlation model of the measured data with the multiple linear regression algorithm and the hybrid particle swarm algorithm to achieve the optimization goal of measurement points. In addition, some scholars have also proposed methods to establish correlation prediction models based on neural networks with the application of deep learning in the field of structural damage identification. In addition, Sahar also builds an improved genetic algorithm through the geometric viewpoint and the numerical forward algorithm of Genetic algorithm (GVGA), and is used to optimize the placement of sensors in the structure, and gets a good effect[4]. For example, Feng[5] proposed a correlation modeling method for the nonlinear behavior of bridge structures with threshold recurrent units of recurrent neural networks; Kaveh A employed backpropagation and radial basis function neural networks to train efficient models for the analysis, design, and prediction of dome displacements. [6].Yang[7] deeply analyzed the correlation characteristics of measurement points in sensors and proposed a recognition method of joint neural network structural state model based on Convolutional Neural Network (CNN) and Gated Recurrent Neural Network (GRU), which provides the basis for optimizing predictions from sensor data.

Through the above research results, it is not difficult to find that the correlation coefficient proposed by most scholars is used to describe the linear relationship between variables. However, potential correlation between variables in actual engineering is far more than linear correlation, and linear measurement indicators cannot satisfy the changes in internal forces of complex structures. Such is the case with large-span space structures. As we know, a large-span space structure has obvious nonlinear properties in the construction process: On the one hand, the space structure will experience a complex time course during its construction, during which it will not only experience various construction loads and construction error factors, but also undergo multiple structural system transformations. Its geometry and boundary conditions show strong time-varying characteristics, so it presents nonlinear characteristics in time series; On the other hand, when the span of a large-span space structure increases, the stiffness decreases and the geometric nonlinearity is obvious. The correlation between the mechanical response of individual members may also show nonlinearity. For example, literature [5] pointed out that the influence of geometric nonlinearity should be considered in the mechanical analysis of construction process of a large-span space structure. When analyzing the construction internal forces of a large-span lattice shell structure, literature [7] found that the nonlinearity had a great influence on the construction internal forces of the members during the construction process. So it is easy to see that the large-span space grid structure has a relatively obvious nonlinear effect in the construction process, that is, the internal force of each member will change nonlinearly with time, loading history and system transformation, and the change law of each member may be different, it is not difficult to predict that the relationship between the internal force of each member may also be nonlinear. At the same time, in the aspect of structural state recognition and prediction, the time-dependent relationship of response monitoring data is often ignored.

To this end, this paper relies on an actual project of a large-span space grid structure, based on the characteristics of certain correlation between structural responses. First, the nonlinear correlation between the stress responses of different members was found by combining the correlation coefficient method and grey correlation method. Then, the appropriate measuring points were selected based on the bond energy algorithm. Finally, the LSTM neural network was used to predict the mechanical response of the relevant measurement points. It is worth nothing that the measurement points optimization method proposed in this paper can not only obtain the nonlinear correlation between the responses of the large-span space grid structure with mathematical method, but also track the entire construction process when predicting the responses of relevant members, and consider the dependence of the correlation between members in the time dimension.

2. Project overview

The central roof of Mall of China adopts an orthogonal truss grid structure in the form of free-form surface. The north-south span of the structure is 139m~108m, and the east-west span is 231m~165m; the height of the grid in the middle region is 5m, and that near the supports is 4~6m. The grid size is 11m×11m. The web members and chord members of the grid adopt spatially intersecting joints, and hollow spherical joints are used to connect all chord members and between chord members and diagonal braces.

In order to improve construction efficiency, the structure adopts a mixed construction method that combines partitioned assembly, cumulative lifting and high-altitude bulk installation. During construction, the central lifting area is divided into three areas, which are cumulatively lifted after ground assembly. The specific construction steps are: after the ground assembly of the first area is completed, it is raised to the height of the second area and connected with the second area that is installed in bulk on the temporary support frames. Then the first and second areas are raised to a certain height as a whole and connected with the third area that is installed in bulk on the support frames. Finally, the three areas are together raised to the designed height as a whole, and spliced with the surrounding hoisting areas at a high altitude. The structure construction process and the overall diagram are shown in Fig.1.Combined with the stress characteristics during the structural construction process, it can be divided into four stages: In the first stage, the support frame in the second area is unloaded, and the first and second areas are lifted as a whole; In the second stage, the support frame in the third area is unloaded, and the first, second and third areas are lifted as a whole; In the third stage, the support frame in the inner and outer rings of the lifting area is unloaded; In the fourth stage, the lifting point is unloaded.

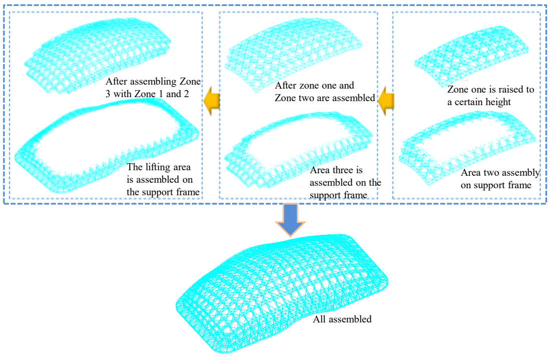

Fig. 1 Central roof steel structure construction process diagram

3. Measurement point optimization method based on response correlation

3.1. Calculation method of response correlation considering multiple construction stages

There are usually two methods to obtain the correlation between the response of the members. One is to find the mechanical relationship between the members within the structure from the mechanical equilibrium and compatibility conditions based on the configuration characteristics of the structure. For the long-span spatial grid structure, due to the large number of member and the high redundancy of the structure, more additional constraints are required to solve the problem. The calculation process is impossible to complete, and in more cases, infinite group solutions will be solved. The other is the use of mathematical statistics, through machine learning sample data, to find out the correlation between different members, its calculation process does not directly depend on the internal mechanical relations of the structure, with operability.

Based on the above reasons, according to the relative change magnitude and trend of structural responses in the construction process, this paper adopts currently commonly used the correlation coefficient method and grey correlation degree to describe the correlation degree between responses and the correlation degree of response change trend over time. In order to measure the similarity of variation and trend between structural responses in the construction process, correlation coefficient method and grey correlation method are used to generate response comprehensive correlation matrix. The calculation process is as follows:

3.1.1. Correlation coefficient method

The correlation coefficient is an indicator that describes the degree of correlation between variables. The Pearson correlation coefficient is commonly used in engineering to measure the similarity between responses. Its calculation principle is:

It is assumed that a structure is divided into α construction stages, and m measuring points are arranged on this structure. If the structural response vector obtained by the i-th (i=1, 2, ⋯, m) measuring point within n time steps of the k-th (k=1, 2, ⋯, α) construction stage is $x_i=[x_i(1), x_i(2), \ldots, x_i(n)]^T$, then the structural response matrix of m measuring points at n time steps in the kth construction stage can be obtained, as shown in formula (1).

$$\boldsymbol{X} = [\boldsymbol{x}_1 \quad \boldsymbol{x}_2 \quad \ldots \quad \boldsymbol{x}_i \quad \ldots \quad \boldsymbol{x}_m] = \begin{bmatrix} x_1(1) & x_2(1) & \ldots & x_i(1) & \ldots & x_m(1) \\ x_1(2) & x_2(2) & \ldots & x_i(2) & \ldots & x_m(2) \\ \vdots & \vdots & \ddots & \vdots & \vdots & \vdots \\ x_1(t) & x_2(t) & \cdots & x_i(t) & \ldots & x_m(t) \\ \vdots & \vdots & \vdots & \vdots & \ddots & \vdots \\ x_1(n) & x_2(n) & \cdots & x_i(n) & \ldots & x_m(n) \end{bmatrix} \tag{1}$$

In the formula, the Pearson correlation coefficient of the response vectors x_i and x_j of any two measuring points i and j in the kth construction stage can be calculated according to formula (2).

$$\begin{aligned} p_{ij} &= \mathrm{cov}(\mathbf{x}_i, \mathbf{x}_j) \big/ \sqrt{\sigma_i \sigma_j} \\ &= E(\mathbf{x}_i - \bar{\mathbf{x}}_i)(\mathbf{x}_j - \bar{\mathbf{x}}_j) \big/ \sqrt{\sigma_i \sigma_j} \end{aligned} \tag{2}$$

Among them, σ_i and σ_j are the variances of the responses at measuring points i and j respectively, which is calculated according to formulas (3) and (4); $\bar{x}_i$ and $\bar{x}_j$ are the response averages of measuring points i and j within n time steps respectively; cov(x_i, x_j) is the covariance of the responses of measuring points i and j, which is calculated according to formula (5).

$$\sigma_i = \frac{1}{n-1}\sum_{t=1}^{n}\left(x_i(t) - \bar{x}_i\right)^2 \tag{3}$$

$$\sigma_i = \frac{1}{n-1}\sum_{t=1}^{n}\left(x_i(t) - \bar{x}_i\right)^2 \tag{4}$$

$$\mathrm{cov}(\mathbf{x}_i, \mathbf{x}_j) = \frac{1}{n-1}\sum_{t=1}^{n}\left(x_i(t) - \bar{x}_i\right)\left(x_j(t) - \bar{x}_j(t)\right) \tag{5}$$

According to formulas (2) to (5), the correlation matrix P of the structural response change of m measuring points at the kth construction stage is obtained, as shown in formula (6).

$$\mathbf{P} = [p_{ij}]_{m\times m} = \begin{bmatrix} p_{11} & p_{12} & \cdots & p_{1j} & \cdots & p_{1m} \\ p_{21} & p_{22} & \cdots & p_{2j} & \cdots & p_{2m} \\ \vdots & \vdots & \ddots & \vdots & \vdots & \vdots \\ p_{i1} & p_{i2} & \cdots & p_{ij} & \cdots & p_{im} \\ \vdots & \vdots & \vdots & \vdots & \ddots & \vdots \\ p_{m1} & p_{m2} & \cdots & p_{mj} & \cdots & p_{mm} \end{bmatrix} \tag{6}$$

The range of Pearson correlation coefficient is $-1 \leqslant p_{ij} \leqslant 1$. If $|p_{ij}|$ is closer to 1, the correlation between measurement points i and j is stronger; If $|p_{ij}|$ is closer to 0, it means that the correlation between measuring points i and j is weaker.

3.1.2. Gray correlation degree

The gray correlation degree describes the relative changes between variables during the development process of the system. If the relative change trends of the two variables during the development process are basically the same, the gray correlation degree is large. On the contrary, if the gray correlation degree is small, it indicates that the relative change trend of the two variables in the development process is inconsistent. This paper adopts B-type gray correlation to measure the similarity of change trends between responses, thereby establishing a correlation matrix of structural response change trends. The calculation principle is:

For any two measuring points i and j in the structure, the responses at the kth construction stage are xi and x_j respectively, and the calculation of their B-type gray correlation degree is as shown in formula (7).

$$r_{ij} = \frac{1}{1 + \frac{1}{n} d_{ij}^{(0)}(t) + \frac{1}{n-1} d_{ij}^{(1)}(t) + \frac{1}{n-2} d_{ij}^{(2)}(t)} \tag{7}$$

$$d_{ij}^{(0)}(t) = \sum_{t=1}^{n}\left|x_i(t) - x_j(t)\right| \tag{8}$$

$$d_{ij}^{(1)}(t)=\sum_{t=1}^{n-1}\left|x_i(t+1)-x_j(t+1)-x_i(t)+x_j(t)\right| \tag{9}$$

$$d_{ij}^{(2)}(t)=\sum_{t=1}^{n-2}\left|\begin{matrix}\left[x_i(t+1)-x_j(t+1)\right]\\ -2\left[x_i(t)-x_j(t)\right]+\left[x_i(t-1)-x_j(t-1)\right]\end{matrix}\right| \tag{10}$$

In the formula, $d_{ij}^{(0)}(t)$ is the overall displacement difference of the response at measuring points i and j; $d_{ij}^{(1)}(t)$ is the overall first-order slope difference of the response of measuring points i and j; $d_{ij}^{(2)}(t)$ is the overall second-order slope difference of the response of measuring points i and j, which is calculated according to formulas (7)~(10) respectively.

According to the above method, the correlation matrix R of the response change trend of m measuring points in the kth construction stage can be calculated as:

$$\mathbf{R}=\left[r_{ij}\right]_{m\times m}=\begin{bmatrix} r_{11} & r_{12} & \cdots & r_{1j} & \cdots & r_{1m}\\ r_{21} & r_{22} & \cdots & r_{2j} & \cdots & r_{2m}\\ \vdots & \vdots & \ddots & \vdots & \vdots & \vdots\\ r_{i1} & r_{i2} & \cdots & r_{ij} & \cdots & r_{im}\\ \vdots & \vdots & \vdots & \vdots & \ddots & \vdots\\ r_{m1} & r_{m2} & \cdots & r_{mj} & \cdots & r_{mm}\end{bmatrix} \tag{11}$$

B-type gray correlation degree rij∈[0,1], if the value of r_{ij} is closer to 1, it means that the correlation between measuring points i and j is greater, and the change trends of the two are more similar; if the value of r_{ij} is closer to 0, indicating that the correlation between measuring points i and j is smaller.

3.1.3. Comprehensive correlation matrix of response

In order to measure the similarity of change magnitude and change trend between structural responses in the construction process, the response comprehensive correlation matrix is generated by combining the change magnitude correlation matrix with the change trend correlation matrix. In order to obtain the response comprehensive correlation matrix effectively, the correlation matrix P and R are treated by setting the correlation threshold, and the equivalent correlation matrix with only 0 and 1 coefficients after binarization is obtained. The specific process is as follows:

First, the similarity threshold λ of the response change magnitude is set, and the correlation matrix P' of the equivalent response changes is obtained as:

$$\mathbf{P}'=\left[p'_{ij}\right]_{m\times m}=\begin{bmatrix} p'_{11} & p'_{12} & \cdots & p'_{1j} & \cdots & p'_{1m}\\ p'_{21} & p'_{22} & \cdots & p'_{2j} & \cdots & p'_{2m}\\ \vdots & \vdots & \ddots & \vdots & \vdots & \vdots\\ p'_{i1} & p'_{i2} & \cdots & p'_{ij} & \cdots & p'_{im}\\ \vdots & \vdots & \vdots & \vdots & \ddots & \vdots\\ p'_{m1} & p'_{m2} & \cdots & p'_{mj} & \cdots & p'_{mm}\end{bmatrix} \tag{12}$$

Among them,

$$p'_{ij}=\begin{cases}1 & \left|p_{ij}\right|\geq\lambda\\ 0 & \left|p_{ij}\right|<\lambda\end{cases} \tag{13}$$

Then, the similarity threshold μ of the response change trend is set, and the correlation matrix R' of the equivalent response change trends is obtained as:

$$\mathbf{R}'=\left[r'_{ij}\right]_{m\times m}=\begin{bmatrix} r'_{11} & r'_{12} & \cdots & r'_{1j} & \cdots & r'_{1m}\\ r'_{21} & r'_{22} & \cdots & r'_{2j} & \cdots & r'_{2m}\\ \vdots & \vdots & \ddots & \vdots & \vdots & \vdots\\ r'_{i1} & r'_{i2} & \cdots & r'_{ij} & \cdots & r'_{im}\\ \vdots & \vdots & \vdots & \vdots & \ddots & \vdots\\ r'_{m1} & r'_{m2} & \cdots & r'_{mj} & \cdots & r'_{mm}\end{bmatrix} \tag{14}$$

Among them,

$$r'_{ij}=\begin{cases}1 & \left|r_{ij}\right|\geq\mu\\ 0 & \left|r_{ij}\right|<\mu\end{cases} \tag{15}$$

According to formulas (14) and (15), the comprehensive correlation matrix of response $\boldsymbol{C}^{(k)}$ of m measuring points in the kth construction stage can be written as:

$$\mathbf{C}^{(k)}=\left[c_{ij}^{(k)}\right]_{m\times m}=\begin{bmatrix} c_{11}^{(k)} & c_{12}^{(k)} & \cdots & c_{1j}^{(k)} & \cdots & c_{1m}^{(k)}\\ c_{21}^{(k)} & c_{22}^{(k)} & \cdots & c_{2j}^{(k)} & \cdots & c_{2m}^{(k)}\\ \vdots & \vdots & \ddots & \vdots & \vdots & \vdots\\ c_{i1}^{(k)} & c_{i2}^{(k)} & \cdots & c_{ij}^{(k)} & \cdots & c_{im}^{(k)}\\ \vdots & \vdots & \vdots & \vdots & \ddots & \vdots\\ c_{m1}^{(k)} & c_{m2}^{(k)} & \cdots & c_{mj}^{(k)} & \cdots & c_{mm}^{(k)}\end{bmatrix} \tag{16}$$

Among them,

$$c_{ij}^{(k)}=\begin{cases}1 & \left(p'_{ij}+r'_{ij}\right)/2=1\\ 0 & \left(p'_{ij}+r'_{ij}\right)/2\neq1\end{cases} \tag{17}$$

In the formula, $c_{ij}^{(k)}$ is the comprehensive correlation coefficient of response of measuring points i and j in the kth construction stage, The coefficient is a Boolean matrix containing only 0 and 1, This coefficient combines the Pearson correlation coefficient and the B-type gray correlation degree. When $c_{ij}^{(k)}=1$, it means that the responses of measuring points i and j in the kth construction stage have strong similarity in the overall time series and change trend; When $c_{ij}^{(k)}=0$, it means that the similarity is weak.

By extracting the response data of m measuring points in each construction stage, correlation analysis was carried out, and the response comprehensive correlation matrix $\boldsymbol{C}^{(1)}$ ~ $\boldsymbol{C}^{(\alpha)}$ of α construction stages could be obtained by calculating according to equation (16). The comprehensive correlation matrix $\boldsymbol{C}$ of structural response in all α construction stages could be further obtained as follows:

$$\boldsymbol{C}=\begin{bmatrix} c_{11} & c_{12} & \cdots & c_{1j} & \cdots & c_{1m}\\ c_{21} & c_{22} & \cdots & c_{2j} & \cdots & c_{2m}\\ \vdots & \vdots & \ddots & \vdots & \vdots & \vdots\\ c_{i1} & c_{i2} & \cdots & c_{ij} & \cdots & c_{im}\\ \vdots & \vdots & \vdots & \vdots & \ddots & \vdots\\ c_{m1} & c_{m2} & \cdots & c_{mj} & \cdots & c_{mm}\end{bmatrix} \tag{18}$$

Among them,

$$c_{ij}=\frac{c_{ij}^{(1)}+c_{ij}^{(2)}+\cdots+c_{ij}^{(k)}+\cdots+c_{ij}^{(\alpha)}}{\alpha} \tag{19}$$

In the formula, c_{ij} is the comprehensive correlation coefficient of response of measuring points i and j in all α construction stages, $c_{ij}\in[0,1]$. When $c_{ij}=1$, the responses of measuring points i and j have strong similarity in the overall time series and change trends of all construction stages, that is, the structural response at the two measuring points has a strong correlation under all construction stages; When $0<c_{ij}<1$, it means that the structural response of the two measuring points only has a strong correlation in certain construction stages; When $c_{ij}=0$, it means that the correlation between the responses of the two measuring points in each construction stage is weak.

3.2. Classification and optimization of measuring points based on bond energy algorithm

According to the comprehensive correlation matrix of response $\boldsymbol{C}$, the correlation of any two measuring points in the entire construction process can be obtained. However, when there are many measuring points, there are many elements in $\boldsymbol{C}$, which makes it difficult to classify the measuring points. Therefore, The Bond Energy Algorithm is introduced to perform cluster analysis on $\boldsymbol{C}$, so that the elements with $c_{ij}=1$ in $\boldsymbol{C}$ are gathered near the diagonal of the matrix, forming a cluster correlation matrix with block characteristics to facilitate the classification of measurement points.

In order to perform effective row-column transformation on the matrix $\boldsymbol{C}$, the matrix $\boldsymbol{C}$ is binary processed again before cluster analysis, and converted into a comprehensive correlation matrix of equivalent response $\boldsymbol{C}'$ with only two elements, 0 and 1, according to formula (20). Then through cluster analysis, all elements in $\boldsymbol{C}'$ are finally restored to their original values.

$$c'_{ij} = \begin{cases} 1 & c_{ij} = 1 \\ 0 & c_{ij} \neq 1 \end{cases} \tag{20}$$

The Bond Energy Algorithm (BEA)[8–11] is a permutation-based algorithm that aggregates similar elements within a matrix through row and column rearrangement as well as segmentation operations, with its core objective being to address the automatic grouping of similar elements in high-dimensional correlation matrices, and its computational procedure is illustrated in Fig.2. BEA takes the equivalent response comprehensive correlation matrix as input and defines the interaction strength between each matrix element and its adjacent elements as "bond energy," and by iteratively adjusting the row and column ordering, it continuously maximizes the global total bond energy(ME);essentially, ME represents the cumulative sum of the bond energies of all elements and reflects the degree of clustering among similar elements within the matrix, and when ME reaches its maximum value, highly correlated elements in the matrix tend to aggregate into diagonal block structures, with each block corresponding to a group of measurement points exhibiting similar response patterns, and the mathematical formulation is given by Equation (21), which accumulates the bond energies between each element and its adjacent elements and employs a coefficient of 1/2 to correct for the double-counting of bidirectional interactions, thereby ensuring that the matrix structure corresponding to the maximum ME directly reflects the "response-similar measurement point groups" in practical engineering applications and achieving a close integration between the algorithmic mechanism and the requirements of structural monitoring.

$$ME = \frac{1}{2}\sum_{i=1}^{m}\sum_{j=1}^{m} c'_{i,j} \times \left(c'_{i,j-1} + c'_{i,j+1} + c'_{i-1,j} + c'_{i+1,j} \right) \tag{21}$$

In the formula,

$c'_{i,j-1}$, $c'_{i,j+1}$, $c'_{i-1,j}$, *and* $c'_{i+1,j}$: the left, right, upper, and lower adjacent elements of the element $c'_{i,j}$, corresponding to the correlation coefficients of adjacent measuring points. $c'_{i,0} = c'_{i,m+1} = c'_{0,j} = c'_{m+1,j} = 0$.

The traditional hierarchical clustering requires constructing an m × m distance matrix and iteratively merging clusters, with each merging operation involving a traversal of the matrix to find the optimal pair, leading to an overall time complexity of O(m³). In contrast, BEA achieves O(m²) complexity. This quadratic vs. cubic difference yields a computational gap of m-fold, directly demonstrating BEA's superiority in large-scale scenarios. As the number of data points m increases, this exponential efficiency advantage solidifies BEA's applicability to high-dimensional engineering datasets.

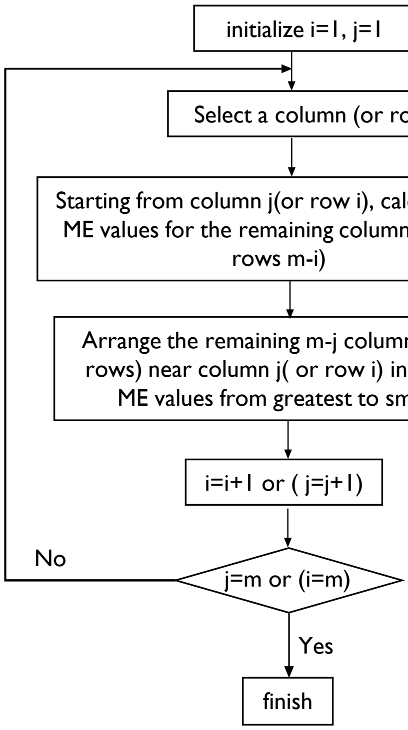

Fig. 2 Flow chart of bond energy algorithm

The comprehensive correlation matrix of response shown in Fig. 3 is taken as an example to illustrate the calculation process of the bond energy algorithm. A total of 10 measurement points from A1 to A10 are shown in Fig.3. The comprehensive correlation matrix of equivalent response is obtained through binary processing based on the comprehensive correlation matrix of response. Then the original values of all coefficients are restored after transformation by the bond energy algorithm, and finally a clustering correlation matrix with block characteristics is obtained.

$$\begin{array}{c} \text{A1} \\ \text{A2} \\ \text{A3} \\ \text{A4} \\ \text{A5} \\ \text{A6} \\ \text{A7} \\ \text{A8} \\ \text{A9} \\ \text{A10} \end{array} \begin{bmatrix} 1 & 0.5 & 0.25 & 0 & 0.5 & 0 & 0.5 & 0.25 & 0.25 & 0.5 \\ 0.5 & 1 & 0.5 & 0.5 & 1 & 0.25 & 0 & 0.25 & 0 & 0 \\ 0.25 & 0.5 & 1 & 1 & 0.25 & 1 & 0 & 0 & 0.5 & 0.25 \\ 0 & 0.5 & 1 & 1 & 0.5 & 1 & 0.25 & 0.5 & 1 & 0.25 \\ 0.5 & 1 & 0.25 & 0.5 & 1 & 0 & 0.5 & 0.25 & 0 & 0.5 \\ 0 & 0.25 & 1 & 1 & 0 & 1 & 0.5 & 0 & 1 & 0.5 \\ 0.5 & 0 & 0 & 0.25 & 0.5 & 0.5 & 1 & 1 & 0.25 & 0 \\ 0.25 & 0.25 & 0 & 0.5 & 0.25 & 0 & 1 & 1 & 0.5 & 1 \\ 0.25 & 0 & 0.5 & 1 & 0 & 1 & 0.25 & 0.5 & 1 & 0.5 \\ 0.5 & 0 & 0.25 & 0.25 & 0.5 & 0.5 & 0 & 1 & 0.5 & 1 \end{bmatrix} \xrightarrow[\text{processing}]{\text{binary}}$$

comprehensive correlation matrix of structural response

$$\begin{array}{c} \text{A1} \\ \text{A2} \\ \text{A3} \\ \text{A4} \\ \text{A5} \\ \text{A6} \\ \text{A7} \\ \text{A8} \\ \text{A9} \\ \text{A10} \end{array} \begin{bmatrix} 1 & 0 & 0 & 0 & 0 & 0 & 0 & 0 & 0 & 0 \\ 0 & 1 & 0 & 0 & 1 & 0 & 0 & 0 & 0 & 0 \\ 0 & 0 & 1 & 1 & 0 & 1 & 0 & 0 & 0 & 0 \\ 0 & 0 & 1 & 1 & 0 & 1 & 0 & 0 & 1 & 0 \\ 0 & 1 & 0 & 0 & 1 & 0 & 0 & 0 & 0 & 0 \\ 0 & 0 & 1 & 1 & 0 & 1 & 0 & 0 & 1 & 0 \\ 0 & 0 & 0 & 0 & 0 & 0 & 1 & 1 & 0 & 0 \\ 0 & 0 & 0 & 0 & 0 & 0 & 1 & 1 & 0 & 1 \\ 0 & 0 & 0 & 1 & 0 & 1 & 0 & 0 & 1 & 0 \\ 0 & 0 & 0 & 0 & 0 & 0 & 0 & 1 & 0 & 1 \end{bmatrix} \xrightarrow{\text{BEA}}$$

comprehensive correlation matrix of equivalent response

$$\begin{array}{c} \text{A1} \\ \text{A2} \\ \text{A5} \\ \text{A3} \\ \text{A4} \\ \text{A6} \\ \text{A9} \\ \text{A7} \\ \text{A8} \\ \text{A10} \end{array} \begin{bmatrix} \boxed{1} & 0.5 & 0.5 & 0.25 & 0 & 0 & 0.25 & 0.5 & 0.25 & 0.5 \\ 0.5 & 1 & 1 & 0.5 & 0.5 & 0.25 & 0 & 0 & 0.25 & 0 \\ 0.5 & 1 & 1 & 0.25 & 0.5 & 0 & 0 & 0.5 & 0.25 & 0.5 \\ 0.25 & 0.5 & 0.25 & 1 & 1 & 1 & 0.5 & 0 & 0 & 0.25 \\ 0 & 0.5 & 0.5 & 1 & 1 & 1 & 1 & 0.25 & 0.5 & 0.25 \\ 0 & 0.25 & 0 & 1 & 1 & 1 & 1 & 0.5 & 0 & 0.5 \\ 0.25 & 0 & 0 & 0.5 & 1 & 1 & 1 & 0.25 & 0.5 & 0.5 \\ 0.5 & 0 & 0.5 & 0 & 0.25 & 0.5 & 0.25 & 1 & 1 & 0 \\ 0.25 & 0.25 & 0.25 & 0 & 0.5 & 0 & 0.5 & 1 & 1 & 1 \\ 0.5 & 0 & 0.5 & 0.25 & 0.25 & 0.5 & 0.5 & 0 & 1 & 1 \end{bmatrix}$$

cluster correlation matrix

Fig. 3 Correlation matrix transformation diagram

According to the arrangement of each block sub-matrix in the clustering correlation matrix, the measuring points at each location can be further divided into five types[12]:①If the block sub-matrix contains only 1 measuring point, then the measuring point is of the first type, such as the measuring point A1 shown in Fig.3;②If the overlapping parts of two or more adjacent block sub-matrices contains only one measuring point, then the measuring point is of the second type, such as the measuring point A8;③If the overlapping parts of two or more adjacent block sub-matrices contain multiple measuring points, then these measuring points are of the third type, such as the measuring points A4 and A6;④If the independent block sub-matrix that has no overlapping parts with the adjacent block sub-matrix contains multiple measuring points, then such measuring points are of the fourth type, such as the measuring points A2 and A5;⑤The remaining measuring points belong to the fifth type, such as the measuring points A3,A7,A9 and A10.

For the first type of measuring points, since the block sub-matrix only contains one measuring point, its structural response information can only be reflected by itself; For a block submatrix containing multiple measurement points, the measurement points included in each block sub-matrix are recorded as cross-correlated measurement points. The structural responses between them all have strong correlation, and their correlations are all greater than the set correlation threshold. An optimal measurement point can be selected in the block sub-matrix to reflect the structural response information of other measuring points in the same sub-matrix. In this way, measurement point optimization can be carried out according to the following principles:

(1) For the first and second types of measuring points, select all of them as points to be measured.

(2) For the third and fourth types of measuring points, respectively calculate the sum of the correlation coefficient values of the rows in the clustering correlation matrix where the structural responses of the corresponding measuring points in each block sub-matrix are located. If the sum of the correlation coefficient values in the row is the largest, it means that the measuring point contains more monitoring information. Therefore, the structural response position with the maximum value is selected as the measurement point to be deployed.

(3) Since the optimal measuring points among the second type of measuring points and the third type of measuring points can already reflect the information of the fifth type of measuring points, the fifth type measuring points are no longer selected as the measuring points to be deployed.

Fig. 3 is optimized according to the above principles. The initial 10 measuring points can be optimized to A1, A4, A5, and A8, with only 4 measuring points.

4. Optimization of construction monitoring measurement points

4.1. Initial plan for measuring points of construction monitoring

In most cases, the stress measurement points during the construction process of long-span spatial structures are mainly arranged in areas based on the structural installation plan, and based on the construction simulation calculation results and structural characteristics, typical representative rod arrangement measurement points are selected. The main principles to be considered are: ① Rods with high stress during construction;②Rods with large stress changes during construction;③Lift the rods near the lifting points;④During the partition installation process, the stress properties of the rods in the connection area may change with the construction process;⑤The upper chord inclined support rod at the peripheral corner end of the lifting unit;⑥Partially symmetrical verification test points;⑦Rods at other important locations.

According to the above principles, the central roof of Mall of China needs to set up a total of 104 measuring points, including 36 in the first lifting area, 22 in the second lifting area, 36 in the third lifting area, and 10 in the hoisting area, as shown in Fig.4. For the convenience of description, the measuring point number is in the form of Wa-b, which is expressed as the bth measuring point in the W-type rod of area a. The rod category W is divided into five types, with U representing the upper chord rod, D representing the lower chord rod, XF representing the oblique web rod, SF representing the vertical web rod, and XZC representing the upper chord inclined support rod.

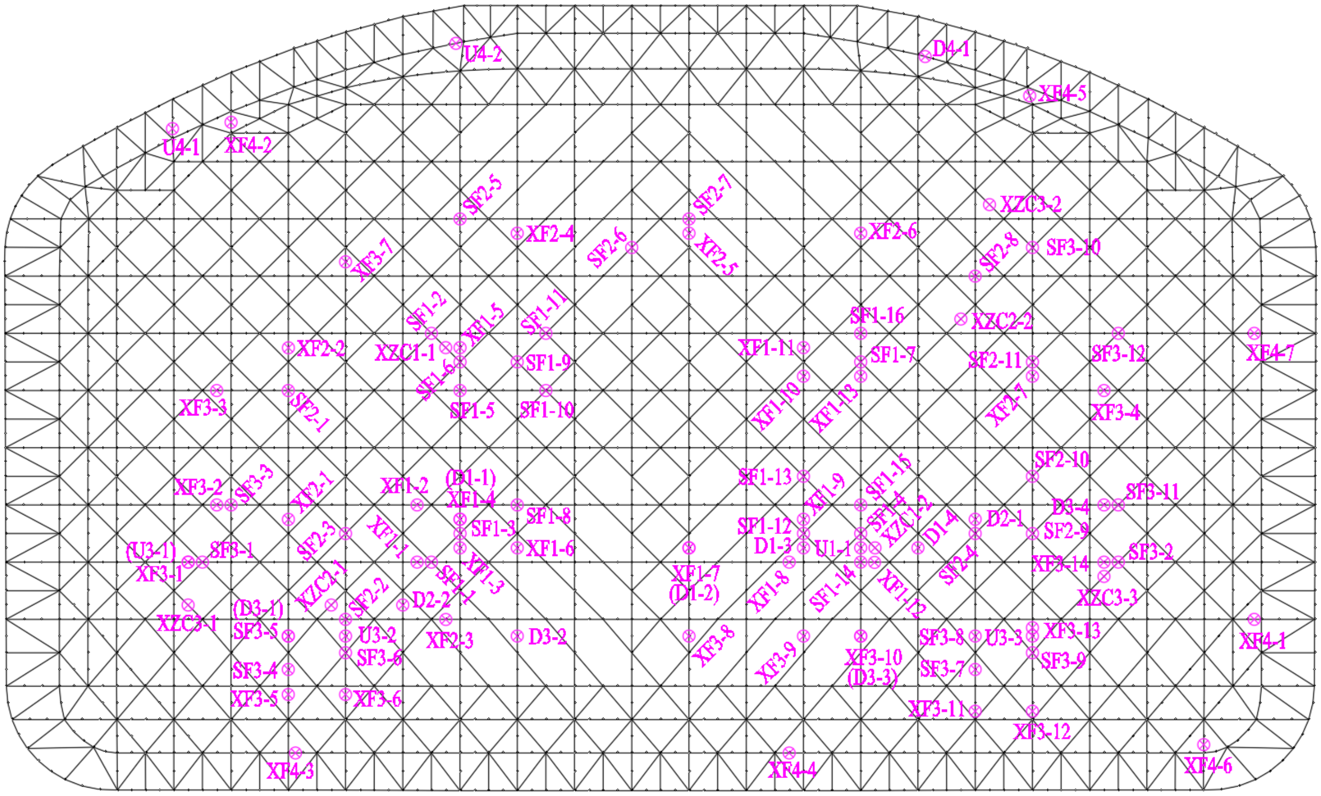

Fig. 4 Stress measuring point layout diagram

4.2. Optimization plan of measurement points

Obviously, the large number of measuring points shown in Fig. 4 brings greater difficulties to construction monitoring. Therefore, 104 measurement points were optimized based on the correlation between structural responses according to the method in Section 2.

According to the construction plan shown in Fig.1, the structural construction process is divided into four stages. Considering that each partition has a sequence of installation, the number of construction stages experienced by each partition is different. Therefore, the correlation analysis and optimal arrangement of the measuring points in each partition are carried out. To this end, the finite element software ANSYS is first used to track and simulate the entire process of structural construction, and structural response data is obtained. Referring to the correlation thresholds used in engineering cases from Reference [13] that are highly similar to the present study in terms of structure and technology, binary correlation matrices were generated by setting λ = μ = 0.6, 0.7, and 0.8, respectively. Based on the method described in Section 2, clustering correlation matrices with block-wise characteristics were calculated for the measurement points in each partition across multiple construction stages under different threshold values. Subsequently, following the classification approach outlined in Section 2.2 for mutually correlated measurement points, the final optimized measurement point configurations corresponding to different thresholds were obtained. The results show that when λ = μ = 0.6, the number of measurement points was reduced by 35; when λ = μ = 0.7, the reduction was 26; and when λ = μ = 0.8, the reduction was 16.

From the perspective of the number of reduced measurement points alone, a lower threshold corresponds to a greater reduction in the number of measurement points. To further select the optimal threshold, the Normalized Root Mean Square Error (NRMSE) was used for comparison. Taking the measured stress data from all 104 measurement points as the complete dataset, the clustering correlation matrix was divided into submatrices based on their distribution, with each submatrix representing a distinct clustering type. From each cluster, the measurement point with the highest sum of correlation coefficients in its row was selected as the representative point. The collection of all representative points formed the simplified measurement point set, where the number of points equaled the number of clusters. The measured data corresponding to these representative points constituted the final simplified dataset. Finally, the Root Mean Square Error (RMSE) between the complete 104 - point dataset and the simplified measurement point set was calculated using Equation (22), followed by the computation of NRMSE as described in Equation (23). The resulting errors for different thresholds are presented in Table 1.

$$\text{RMSE} = \sqrt{\frac{1}{n}\sum_{t=1}^{n}(x_t - \hat{x}_t)^2} \tag{22}$$

In the above formula:

n: the number of data samples;

x_t: the true value (measured stress data from the complete dataset);

$\hat{x}_t$: the predicted value (representative value from the simplified measurement point set, e.g., data from representative points selected via clustering).

$$NRMSE = \frac{RMSE}{\bar{y}} \times 100\%, \bar{y} = \frac{1}{n}\sum_{i=1}^{n} y_i \tag{23}$$

The core logic for selecting the optimal threshold among different threshold corresponding stress error and measurement point quantity results is to maximize the simplification efficiency on the premise of meeting the accuracy requirements. As can be seen from the table1, although the number of reduced measurement points is the largest when the threshold is 0.6, its NRMSE exceeds the engineering allowed error (5%). The main reason is that a relatively small threshold causes more measurement points to be judged as redundant when their correlation coefficients exceed the threshold. Eventually, many weakly correlated measurement points are included, resulting in large data restoration errors. When the threshold is 0.8, only a very small number of extremely strongly correlated measurement points are judged as redundant, and the number of reducible measurement points is small. Considering both the number of reduced measurement points and the NRMSE, λ = μ = 0.7 is the optimal choice.

Table 1
Optimization Results Under Different Thresholds

Threshold λ、μ	Decrease in sensor count	NRMSE
0.6	35	0.0753
0.7	26	0.0476
0.8	16	0.0432

Fig.5 shows the clustering correlation matrix obtained by cluster analysis using BEA after binarization when λ = μ = 0.7. Then, the mutually - correlated measurement points are classified according to Section 2.2, as shown in Table 2.

U1-1	1	0.5	0.25	0.5	0.5	0.5	0.25	0.25	0.25	0.25	0.25	0.25	0.25	0.25	0.5	0.5	0.25	0.25	0.25	0.25	0	0	0	0	0.25	0	0.5	0.25	0.5	0.25	0	0	0.25	0	0.5	0.5
D1-1	0.5	1	1	0.25	0.25	0.5	0.5	0.25	0.75	0.25	0.25	0.25	0.25	0.25	0.25	0	0.5	0.25	0.25	0.5	0	0	0.25	0.25	0.5	0	0.25	0.75	0.5	0.25	0.25	0	0.25	0.25	0	0.5
SF1-8	0.25	1	1	0.25	0.25	0.25	0.25	0.25	0.5	0.25	0.25	0.25	0.25	0.25	0.25	0	0.5	0.25	0.25	0.5	0	0	0.25	0	0.5	0	0.25	0.75	0.5	0.25	0.25	0	0.25	0	0.25	0.5
D1-2	0.5	0.25	0.25	1	0.5	0.75	0.25	0.25	0.25	0.5	0.25	0.25	0.5	0.5	0.25	0	0.25	0.25	0.5	0.25	0	0.25	0.25	0.25	0.25	0	0.25	0	0.25	0.75	0.75	0.5	0.25	0	0	0.25
D1-3	0.5	0.25	0.25	0.5	1	0.5	0.5	0.25	0.5	0	0.5	0.5	0.5	0.5	0.5	0.5	0.25	0.75	0.5	0.25	0.25	0	0	0	0.25	0.25	0.25	0.25	0.25	0.5	0.25	0.25	0.25	0	0.5	0.5
D1-4	0.5	0.5	0.25	0.75	0.5	1	1	1	0.75	0.5	0.25	0.25	0.25	0.25	0.5	0	0.25	0.25	0.25	0.5	0	0	0.25	0.25	0.5	0	0.5	0.25	0.5	0.5	0.5	0.25	0.5	0	0	0.5
SF1-13	0.25	0.5	0.25	0.25	0.5	1	1	1	0.75	0.5	0.25	0.25	0.25	0.25	0.5	0	0.25	0.25	0.25	0.5	0	0	0.5	0	0.5	0	0.5	0	0.5	0.75	0.5	0.5	0.5	0	0	0.5
XF1-1	0.25	0.25	0.25	0.25	0.25	1	1	1	1	1	0.25	0.25	0.25	0.25	0.25	0	0.25	0.25	0.25	0.5	0	0.25	0	0	0.25	0	0.5	0	0.25	0.75	0.5	0.5	0.5	0	0	0.5
XF1-6	0.25	0.75	0.5	0.25	0.5	0.75	0.75	1	1	0.75	0.25	0.25	0.25	0	0.25	0	0.25	0.25	0.25	0.5	0	0	0	0	0.25	0	0.5	0	0.25	0.5	0.5	0.25	0.5	0	0.25	0.5
XF1-11	0.25	0.25	0.25	0.5	0	0.5	0.5	1	0.75	1	0.25	0.25	0.25	0.25	0.25	0	0.25	0.25	0.25	0.25	0	0	0.25	0.25	0.25	0	0.5	0	0.25	0.75	0.75	0.75	0.5	0	0	0.5
SF1-9	0.25	0.25	0.25	0.25	0.5	0.25	0.25	0.25	0.25	0.25	1	1	1	0.5	0.5	0.25	0.25	0.5	0.5	0.25	0.5	0	0.25	0.5	0.25	0.25	0.25	0	0.25	0.5	0.25	0	0.25	0	0	0.25
SF1-1	0.25	0.25	0.25	0.25	0.5	0.25	0.25	0.25	0.25	0.25	1	1	1	1	0.5	0	0.25	0.5	0.25	0.25	0.25	0	0	0.25	0.25	0.25	0.25	0	0.25	0.5	0.25	0	0.25	0	0	0.75
SF1-7	0.25	0.25	0.25	0.5	0.5	0.25	0.25	0.25	0.25	0.25	1	1	1	1	0.5	0.25	0.25	0.75	0.5	0.25	0.25	0	0.25	0.5	0.25	0.75	0.25	0	0.25	0.25	0.25	0.25	0.25	0	0.25	0.5
XF1-9	0.25	0.25	0.25	0.5	0.5	0.25	0.25	0.25	0	0.25	0.5	1	1	1	1	0	0.25	0.5	0.75	0.25	0	0	0.25	0.5	0.25	0.5	0.25	0	0.25	0.25	0.25	0.25	0.25	0.25	0	0.5
XF1-10	0.5	0.25	0.25	0.25	0.5	0.5	0.5	0.25	0.25	0.25	0.5	0.5	0.5	1	1	0.25	0.25	0.5	0.5	0.25	0.25	0	0.25	0	0.25	0.25	0.25	0.25	0.5	0.5	0.5	0	0.25	0	0.75	0.75
SF1-2	0.5	0	0	0	0.5	0	0	0	0	0	0.25	0	0.25	0	0.25	1	0.25	0.25	0.5	0	0.75	0.25	0	0.25	0	0.25	0	0	0	0.25	0.75	0.5	0	0	0.25	0.25
SF1-3	0.25	0.5	0.5	0.25	0.25	0.25	0.25	0.25	0.25	0.25	0.25	0.25	0.25	0.25	0.25	0.25	1	0.5	0.25	0.5	0	0	0	0	0.25	0	0.25	0.25	0.75	0.25	0.25	0	0.25	0	0.25	0.25
SF1-4	0.25	0.25	0.25	0.25	0.75	0.25	0.25	0.25	0.25	0.25	0.5	0.5	0.75	0.5	0.5	0.25	0.5	1	1	0.5	0.25	0	0.25	0.25	0.25	0.5	0.25	0	0.25	0.5	0.5	0.25	0.25	0.25	0.5	0.5
SF1-14	0.25	0.25	0.25	0.5	0.5	0.25	0.25	0.25	0.25	0.25	0.5	0.25	0.5	0.75	0.5	0.5	0.25	1	1	0.25	0.25	0	0.25	0.25	0.25	0.25	0.25	0	0.25	0.25	0.25	0	0.25	0	0.5	0.5
SF1-5	0.25	0.5	0.5	0.25	0.25	0.5	0.5	0.5	0.5	0.25	0.25	0.25	0.25	0.25	0.25	0	0.5	0.5	0.25	1	0	0	0.5	0.25	0.5	0	0.25	0	0.25	0.25	0.25	0.25	0.25	0	0	0.25
SF1-6	0	0	0	0	0.25	0	0	0	0	0	0.5	0.25	0.25	0	0.25	0.75	0	0.25	0.25	0	1	0.25	0	0.25	0	0.5	0	0	0	0.25	0.5	0.5	0	0.25	0.25	0
SF1-10	0	0	0	0.25	0	0	0	0.25	0	0	0	0	0	0	0	0.25	0	0	0	0	0.25	1	1	0	0	0	0	0	0	0	0.25	0	0	0.5	0.25	0
SF1-11	0	0.25	0.25	0.25	0	0.25	0.5	0	0	0.25	0.25	0	0.25	0.25	0.25	0	0	0.25	0.25	0.5	0	1	1	0.25	0.25	0.25	0.25	0	0.25	0.25	0.25	0.25	0.25	0.25	0	0.25
SF1-12	0	0.25	0	0.25	0	0.25	0	0	0	0.25	0.5	0.25	0.5	0.5	0	0.25	0	0.25	0.25	0.25	0.25	0	0.25	1	0	0.25	0.25	0	0	0.25	0.5	0.25	0.25	0	0	0
SF1-15	0.25	0.5	0.5	0.25	0.25	0.5	0.5	0.25	0.25	0.25	0.25	0.25	0.25	0.25	0.25	0	0.25	0.25	0.25	0.5	0	0	0.25	0	1	0	0.25	0.25	0.25	0.25	0.25	0	0.25	0	0	0.5
SF1-16	0	0	0	0	0.25	0	0	0	0	0	0.25	0.25	0.75	0.5	0.25	0.25	0	0.5	0.25	0	0.5	0	0.25	0.25	0	1	0	0	0	0	0	0	0	0	0.25	0
XF1-2	0.5	0.25	0.25	0.25	0.25	0.5	0.5	0.5	0.5	0.5	0.25	0.25	0.25	0.25	0.25	0	0.25	0.25	0.25	0.25	0	0	0.25	0.25	0.25	0	1	0	0.25	0.5	0.5	0.25	0.5	0	0	0.5
XF1-3	0.25	0.75	0.75	0	0.25	0.25	0	0	0	0	0	0	0	0	0.25	0	0.25	0	0	0	0	0	0	0	0.25	0	0	1	0.25	0	0	0	0	0	0.5	0.25
XF1-4	0.5	0.5	0.5	0.25	0.25	0.5	0.5	0.25	0.25	0.25	0.25	0.25	0.25	0.25	0.5	0	0.75	0.25	0.25	0.25	0	0	0.25	0	0.25	0	0.25	0.25	1	0.25	0.25	0	0.25	0	0	0.25
XZC1-1	0.25	0.25	0.25	0.75	0.5	0.5	0.75	0.75	0.5	0.75	0.5	0.5	0.25	0.25	0.5	0.25	0.25	0.5	0.25	0.25	0.25	0	0.25	0.25	0.25	0	0.5	0	0.25	1	1	0.25	0.5	0	0.25	0.75
XF1-5	0	0.25	0.25	0.75	0.25	0.5	0.5	0.5	0.5	0.75	0.25	0.25	0.25	0.25	0.5	0.75	0.25	0.5	0.25	0.25	0.5	0.25	0.25	0.5	0.25	0	0.5	0	0.25	1	1	1	0.5	0	0	0.5
XF1-12	0	0	0	0.5	0.25	0.25	0.5	0.5	0.25	0.75	0	0	0.25	0.25	0	0.5	0	0.25	0	0.25	0.5	0	0.25	0.25	0	0	0.25	0	0	0.25	1	1	0.5	0.25	0	0.25
XF1-7	0.25	0.25	0.25	0.25	0.25	0.5	0.5	0.5	0.5	0.5	0.25	0.25	0.25	0.25	0.25	0	0.25	0.25	0.25	0.25	0	0	0.25	0.25	0.25	0	0.5	0	0.25	0.5	0.5	0.5	1	0	0	0.25
XF1-8	0	0.25	0	0	0	0	0	0	0	0	0	0	0	0.25	0	0	0	0.25	0	0	0.25	0.5	0.25	0	0	0	0	0	0	0	0	0.25	0	1	0	0
XF1-13	0.5	0	0.25	0	0.5	0	0	0	0.25	0	0	0	0.25	0	0.75	0.25	0.25	0.5	0.5	0	0.25	0.25	0	0	0	0.25	0	0.5	0	0.25	0	0	0	0	1	0.5
XZC1-2	0.5	0.5	0.5	0.25	0.5	0.5	0.5	0.5	0.5	0.5	0.25	0.75	0.5	0.5	0.75	0.25	0.25	0.5	0.5	0.25	0	0	0.25	0	0.5	0	0.5	0.25	0.25	0.75	0.5	0.25	0.25	0	0.5	1

(a) Promoted first district (Contains 4 phases)

D2-1	1	0.5	0.25	0.5	0.25	0.5	0.25	0.25	0	0.25	0	0.25	0	0.5	0	0	0.25	0.25	0	0.25	0.5	0.25
D2-2	0.5	1	0.5	0.75	0.75	0.75	0.5	0.25	0	0.25	0.5	0	0	0.5	0.25	0.25	0.5	0.25	0.75	0	0.25	0.25
SF2-1	0.25	0.5	1	1	0.5	0.75	0.5	0.5	0	0.5	0.5	0.5	0.25	0.75	0.25	0.25	0.75	0.75	0.5	0.25	0.5	0.25
XF2-4	0.5	0.75	1	1	1	0.25	0.5	0.25	0.25	0.75	0.5	0.5	0.25	0.5	0.25	0.25	0.25	0.75	0.5	0.25	0.25	0.25
XF2-3	0.25	0.75	0.5	1	1	0.25	0.25	0.25	0.25	0.25	0.25	0.5	0.25	0.5	0.25	0.25	0.5	0.25	0.5	0	0	0.25
SF2-2	0.5	0.75	0.75	0.25	0.25	1	0.25	0	0	0.5	0.25	0	0.25	0.75	0	0.25	0.5	0.5	0.25	0.25	0.25	0.25
SF2-3	0.25	0.5	0.5	0.5	0.25	0.25	1	0.75	0.25	0.5	0.25	0.75	0.5	0.5	0.25	0.25	0.25	0	0.25	0.25	0.5	0.25
SF2-4	0.25	0.25	0.5	0.25	0.25	0	0.75	1	0.25	0.25	0.25	0.5	0.5	0.5	0.25	0.25	0.25	0	0.25	0	0.25	0.25
SF2-5	0	0	0	0.25	0.25	0	0.25	0.25	1	0.75	0.25	0.25	0.25	0.25	0	0	0.25	0.25	0	0.25	0.5	0.5
SF2-6	0.25	0.25	0.5	0.75	0.25	0.5	0.5	0.25	0.75	1	0.75	0.25	0.5	0.5	0.25	0.25	0.5	0.25	0.25	0.5	0.5	0.5
SF2-7	0	0.5	0.5	0.5	0.25	0.25	0.25	0.25	0.25	0.75	1	0.25	0.25	0.5	0	0.25	0.25	0.25	0.25	0.25	0.75	0.25
SF2-8	0.25	0	0.5	0.5	0.5	0	0.75	0.5	0.25	0.25	0.25	1	0.5	0.5	0.25	0.25	0.25	0	0.25	0.5	0.25	0.5
SF2-9	0	0	0.25	0.25	0.25	0.25	0.5	0.5	0.25	0.5	0.25	0.5	1	0.25	0.25	0.25	0.25	0.25	0.25	0.5	0	0.5
SF2-10	0.5	0.5	0.75	0.5	0.5	0.75	0.5	0.5	0.25	0.5	0.5	0.5	0.25	1	0.25	0.25	0.5	0.75	0.5	0.25	0.25	0.25
SF2-11	0	0.25	0.25	0.25	0.25	0	0.25	0.25	0	0.25	0	0.25	0.25	0.25	1	0.25	0.25	0	0.25	0.5	0	0
XF2-1	0	0.25	0.25	0.25	0.25	0.25	0.25	0.25	0	0.25	0.25	0.25	0.25	0.25	0.25	1	0.25	0.25	0.25	0.25	0	0.25
XF2-2	0.25	0.5	0.75	0.25	0.5	0.5	0.25	0.25	0.25	0.5	0.25	0.25	0.25	0.5	0.25	0.25	1	0.25	0.25	0	0.25	0
XF2-5	0.25	0.25	0.75	0.75	0.25	0.5	0	0	0.25	0.25	0.25	0	0.25	0.75	0	0.25	0.25	1	0.25	0.25	0.25	0
XF2-6	0	0.75	0.5	0.5	0.5	0.25	0.25	0.25	0	0.25	0.25	0.25	0.25	0.5	0.25	0.25	0.25	0.25	1	0	0	0
XF2-7	0.25	0	0.25	0.25	0	0.25	0.25	0	0.25	0.5	0.25	0.5	0.5	0.25	0.5	0.25	0	0.25	0	1	0.25	0.75
XZC2-1	0.5	0.25	0.5	0.25	0	0.25	0.5	0.25	0.5	0.5	0.75	0.25	0	0.25	0	0	0.25	0.25	0	0.25	1	0.25
XZC2-2	0.25	0.25	0.25	0.25	0.25	0.25	0.25	0.25	0.5	0.5	0.25	0.5	0.5	0.25	0	0.25	0	0	0	0.75	0.25	1

(b) Promote the second zone (Contains 4 phases)

U3-1	1	0.33	0.67	0	0	0	0.33	0.33	0.33	0.33	0.33	0	0.33	0	0	0.33	0.33	0.33	0	0	0.33	0.67	0	0	0	0.33	0.67	0.33	0.33	0	0	0.33	0	0	0	0.33
U3-2	0.33	1	0.67	0.33	0	0	0	0	0	0	0.33	0	0	0	0	0.33	0	0	0	0	0	0	0	0	0	0	0.33	0	0	0	0	0	0	0	0	0
U3-3	0.67	0.67	1	0	0	0	0	0	0	0.67	0.67	0	0.33	0	0	0.33	0.33	0.33	0	0	0	0.33	0	0	0	0	0.33	0.67	0	0	0	0	0	0.33	0	0.33
D3-1	0	0.33	0	1	0	0.33	0.33	0	0	0	0	0.33	0	0.33	0.33	0	0	0	0.33	0	0	0	0	0	0	0	0	0	0	0.33	0	0	0	0.33	0	0
D3-2	0	0	0	0	1	1	0.33	0	0	0	0	0	0	0.33	0	0	0.33	0.33	0.67	0	0.67	0	0	0	0	0	0	0	0	0.67	0	0	0	0	0.33	0
D3-3	0	0	0	0.33	1	1	0.33	0	0	0	0	0	0	0.33	0.67	0	0	0	0.67	0	0.67	0	0	0	0	0	0	0	0	0.67	0.67	0	0	0.67	0	0
D3-4	0.33	0	0	0.33	0.33	0.33	1	0	0	0	0	0	0	0	0.33	0	0	0	0.67	0	0.33	0.33	0	0	0.33	0	0	0	0	0.33	0.33	0	0.33	0.33	0	0.33
SF3-1	0.33	0	0	0	0	0	0	1	1	1	0	0	0	0	0	0.33	0.67	0.33	0	0.33	0.33	0.33	0.33	0.33	0	0.33	0.33	0.33	0.67	0	0	0.67	0	0	0	0
SF3-2	0.33	0	0	0	0	0	0	1	1	0.67	0	0	0.33	0	0	0.33	0.67	0.67	0	0.67	0	0.33	0.33	0.67	0	0	0.33	0.33	0.33	0	0	0.67	0.33	0	0	0
SF3-11	0.33	0	0.67	0	0	0	0	1	0.67	1	1	0	0.33	0	0	0.33	0.67	0.67	0	0.67	0.33	0.33	0	0.67	0	0.33	0.33	0.33	0.33	0	0	0.33	0.33	0	0	0
SF3-12	0.33	0.33	0.67	0	0	0	0	0	0	1	1	0	0	0	0	0.33	0.67	0	0	0.33	0	0	0	0.67	0	0	0	0	0	0	0	0	0	0.33	0	0.33
SF3-3	0	0	0	0.33	0	0	0	0	0	0	0	1	0	0	0	0	0	0	0	0	0.33	0	0	0	0	0	0	0	0	0	0	0	0	0	0	0
SF3-4	0.33	0	0.33	0	0	0	0	0	0.33	0.33	0	0	1	0.33	0.33	0.67	0.33	0.33	0	0	0	0.33	0	0.33	0.33	0.33	0.33	0.33	0	0	0	0.33	0	0	0	0
SF3-5	0	0	0	0.33	0.33	0.33	0	0	0	0	0	0	0.33	1	1	0	0	0	0.33	0	0	0	0	0	0.33	0	0	0	0	0.33	0.33	0	0	0.33	0	0
XF3-6	0	0	0	0.33	0	0.67	0.33	0	0	0	0	0	0.33	1	1	0.33	0	0	0.33	0	0.33	0	0	0	0.67	0	0	0	0	0.67	0.67	0	0	0.33	0	0
SF3-6	0.33	0.33	0.33	0	0	0	0	0.33	0.33	0.33	0.33	0	0.67	0	0.33	1	0.67	0.67	0	0	0	0.33	0	0.33	0.33	0	0.33	0.67	0.33	0	0	0.33	0.33	0	0	0
SF3-7	0.33	0	0.33	0	0.33	0	0	0.67	0.67	0.67	0.67	0	0.33	0	0	0.67	1	1	0	0.67	0	0.33	0	0.33	0	0.33	0.33	0.33	0.33	0.33	0.33	0.33	0.33	0	0	0
SF3-9	0.33	0	0.33	0	0.33	0	0	0.33	0.67	0.67	0	0	0.33	0	0	0.67	1	1	0	0.33	0	0.33	0	0.67	0	0	0.33	0.67	0	0.33	0	0.67	0.67	0	0	0
SF3-8	0	0	0	0.33	0.67	0.67	0.67	0	0	0	0	0	0	0.33	0.33	0	0	0	1	0	0.67	0	0	0	0.33	0	0	0	0	0.67	0.67	0	0	0.33	0	0
SF3-10	0	0	0	0	0	0	0	0.33	0.67	0.67	0.33	0	0	0	0	0	0.67	0.33	0	1	0	0	0.67	0.33	0	0.33	0	0.67	0.33	0	0	0.33	0.33	0	0	0
XF3-1	0.33	0	0	0	0.67	0.67	0.33	0.33	0	0.33	0	0.33	0	0	0.33	0	0	0	0.67	0	1	0	0	0	0	0	0	0	0	0.67	0.67	0	0	0.33	0	0
XF3-2	0.67	0	0.33	0	0	0	0.33	0.33	0.33	0.33	0	0	0.33	0	0	0.33	0.33	0.33	0	0	0	1	0.33	0.33	0	0	0.33	0.33	0	0	0	0.67	0.33	0	0.33	0.33
XF3-3	0	0	0	0	0	0	0	0.33	0.33	0	0	0	0	0	0	0	0	0	0	0.67	0	0.33	1	0.33	0	0	0.33	0.33	0	0	0	0.33	0.33	0	0	0
XF3-4	0	0	0	0	0	0	0	0.33	0.67	0.67	0.67	0	0.33	0	0	0.33	0.33	0.67	0	0.33	0	0.33	0.33	1	0	0	0.33	0.33	0	0	0	0.67	0.67	0	0	0
XF3-5	0	0	0	0	0	0	0.33	0	0	0	0	0	0.33	0.33	0.67	0.33	0	0	0.33	0	0	0	0	0	1	0	0	0	0	0.33	0.67	0	0	0	0	0
XF3-7	0.33	0	0	0	0	0	0	0.33	0	0.33	0	0	0.33	0	0	0	0.33	0	0	0.33	0	0	0	0	0	1	0.33	0.33	0.33	0	0	0	0	0	0	0
XF3-8	0.67	0.33	0.33	0	0	0	0	0.33	0.33	0.33	0	0	0.33	0	0	0.33	0.33	0.33	0	0	0	0.33	0.33	0.33	0	0.33	1	0.33	0.33	0	0	0.33	0	0	0	0
XF3-9	0.33	0	0.67	0	0	0	0	0.33	0.33	0.33	0	0	0.33	0	0	0.67	0.33	0.67	0	0.67	0	0.33	0.33	0.33	0	0.33	0.33	1	1	0	0	0.67	0	0	0	0
XF3-10	0.33	0	0	0	0	0	0	0.67	0.33	0.33	0	0	0	0	0	0.33	0.33	0	0	0.33	0	0	0	0	0	0.33	0.33	1	1	0	0	0.67	0.33	0	0	0
XF3-11	0	0	0	0.33	0.67	0.67	0.33	0	0	0	0	0	0	0.33	0.67	0	0.33	0.33	0.67	0	0.67	0	0	0	0.33	0	0	0	0	1	1	0	0	0.33	0	0
XF3-12	0	0	0	0	0	0.67	0.33	0	0	0	0	0	0	0.33	0.67	0	0.33	0	0.67	0	0.67	0	0	0	0.67	0	0	0	0	1	1	0	0	0	0	0
XF3-13	0.33	0	0	0	0	0	0	0.67	0.67	0.33	0	0	0.33	0	0	0.33	0.33	0.67	0	0.33	0	0.67	0.33	0.67	0	0	0.33	0.67	0.67	0	0	1	0.67	0	0	0.33
XF3-14	0	0	0	0	0	0	0.33	0	0.33	0.33	0	0	0	0	0	0.33	0.33	0.67	0	0.33	0	0.33	0.33	0.67	0	0	0	0	0.33	0	0	0.67	1	0	0	0.33
XZC3-1	0	0	0.33	0.33	0	0.67	0.33	0	0	0	0.33	0	0	0.33	0.33	0	0	0	0.33	0	0.33	0	0	0	0	0	0	0	0	0.33	0	0	0	1	0	0
XZC3-2	0	0	0	0	0.33	0	0	0	0	0	0	0	0	0	0	0	0	0	0	0	0	0.33	0	0	0	0	0	0	0	0	0	0	0	0	1	0.67
XZC3-3	0.33	0	0.33	0	0	0	0.33	0	0	0	0.33	0	0	0	0	0	0	0	0	0	0	0.33	0	0	0	0	0	0	0	0	0	0.33	0.33	0	0.67	1

(c) Promote the third zone (Contains 3 phases)

U4-2	1	1	1	1	0.5	0.5	1	0.5	0	0.5
XF4-4	1	1	1	1	0.5	0.5	0.5	0.5	0.5	0.5
XF4-7	1	1	1	1	0.5	0.5	0.5	0.5	0	0.5
U4-1	1	1	1	1	1	1	0.5	0.5	0.5	0.5
XF4-2	0.5	0.5	0.5	1	1	1	0.5	0.5	0.5	0.5
XF4-5	0.5	0.5	0.5	1	1	1	0.5	0.5	0.5	0.5
D4-1	1	0.5	0.5	0.5	0.5	0.5	1	1	0	0.5
XF4-1	0.5	0.5	0.5	0.5	0.5	0.5	1	1	0	0.5
XF4-3	0	0.5	0	0.5	0.5	0.5	0	0	1	0
XF4-6	0.5	0.5	0.5	0.5	0.5	0.5	0.5	0.5	0	1

(d) Bulk area (Contains 2 phases)

Fig. 5 Cluster correlation matrix of zone measuring points

Table 2
Test point classification results table

Station category	Station number
Test points of the first kind	U1-1、D1-2、D1-3、SF1-2、SF1-3、SF1-5、、SF1-6、SF1-12、SF1-15、SF1-16、XF1-2、、XF1-3、XF1-4、XF1-7、XF1-8、XF1-11、XF1-13、XZC1-2、D2-1、D2-2、SF2-2、SF2-3、SF2-4、SF2-5、SF2-6、SF2-7、SF2-8、SF2-9、、SF2-10、SF2-11、XF2-1、XF2-2、XF2-5、XF2-6、XF2-7、XZC2-1、XZC2-2、U3-1、、U3-2、U3-3、D3-1、D3-4、SF3-3、SF3-4、、SF3-6、SF3-8、SF3-10、XF3-1、XF3-2、XF3-3、XF3-4、XF3-5、XF3-7、XF3-8、XF3-13、XF3-14、XZC3-1、XZC3-2、XZC3-3、XF4-3、XF4-6
The second type of measuring point	XF1-1、XF1-5、XF1-9、XF2-4、U4-1
The third type of measuring point	{SF1-1，SF1-7}
The fourth type of measuring point	{D1-1，SF1-8}、{SF1-4，SF1-14}、{SF1-10，SF1-11}、{D3-2，D3-3}、{SF3-1，SF3-2}、{SF3-5，XF3-6}、{SF3-7，SF3-9}、{SF3-11，SF3-12}、{XF3-9，XF3-10}、{XF3-11，XF3-12}、{D4-1，XF4-1}
The fifth test point	D1-4、SF1-9、SF1-13、XF1-6、XF1-10、XF1-12、XZC1-1、SF2-1、XF2-3、U4-2、XF4-2、XF4-4、XF4-5、XF4-7

Combining Fig.4 and Fig.5, it can be found that the cross-correlated measuring points in each block sub-matrix are close to symmetrical or adjacent relationship in spatial position. It shows that there is indeed a large correlation between the structural response information of certain spatial symmetry positions and adjacent positions, which illustrates the effectiveness of the correlation analysis method to a certain extent.

According to the aforementioned layout principle of optimal measuring points, except that the first and second types of measuring points are directly determined as the optimal measuring points. One measuring point in each block sub-matrix of the third and fourth types will be selected as the optimal measuring point. After calculating and comparing the structural response of the corresponding measuring points in each block submatrix and the sum of the correlation coefficients of the rows in the clustering correlation matrix, D1-1, SF1-4, SF1-7, SF1-11, D3-3, SF3-2, SF3-7, SF3-11, XF3-6, XF3-9, XF3-11 and D4-1 are the optimal measuring points. In addition to the auto-correlated measuring points, the measuring points selected from the cross-correlated measuring points and their corresponding related measuring points are shown in Table 3. Furthermore, the number of measurement points after final optimization was reduced to 78, as shown in Fig.6. Compared with the initial plan, it was reduced by 25%.

Although the measurement point reduction ratio in this study is lower than those reported in Ref.[1–4], a 25% reduction still achieves satisfactory results for the central roof steel structure of Mall of China, which features complex spatial geometry, is subjected to diverse loading conditions, and requires a comprehensive evaluation of correlations among all structural points; unlike previous studies in the literature that primarily focus on symmetric structures, single-type loading scenarios, or the optimization of localized components, this research targets the entire roof system — a structure characterized by relatively weak mechanical correlations among its components and greater challenges in optimization, and in practical applications, the extent of measurement point reduction should be determined through a trade-off between monitoring accuracy, data integrity, and implementation cost, rather than pursuing an excessively high reduction ratio in isolation; by integrating binary correlation matrix processing with BEA, an approach validated in Ref.[2]and [12], the proposed method achieves efficient measurement point reduction while maintaining monitoring effectiveness, thereby demonstrating its suitability for structural health monitoring in complex structural systems.

It is noteworthy that both the current study and the research in Ref. [13] focus on small-to-medium spatial structures, in which BEA and clustering algorithms demonstrate efficient optimization of modal measurement points. For super-large structures, however, the original BEA algorithm faces dual bottlenecks in computational complexity and dense matrix memory consumption, which may compromise feasibility due to excessive runtime or memory overflow. The scalability of the algorithm can be improved through the use of sparse matrices, parallel computing, and divide-and-conquer strategies. While the proposed method has been validated for medium-scale structures, its applicability to super-large structures relies on these optimization techniques as a direction for future research.

Table 3
Measuring point layout points and corresponding relevant measuring point information table

Test point layout point	Corresponding correlation measuring points	Test point layout point	Corresponding correlation measuring points
D1-1	SF1-8	SF3-2	SF3-1
SF1-4	SF1-14	SF3-7	SF3-9
SF1-7	SF1-1、SF1-9、XF1-9	SF3-11	SF3-12
SF1-11	SF1-10	XF3-6	SF3-5
XF1-1	D1-4、SF1-13、XF1-6	XF3-9	XF3-10
XF1-5	XZC1-1、XF1-12	XF3-11	XF3-12
XF1-9	SF1-1、SF1-7、XF1-10	U4-1	U4-2、XF4-4、XF4-7、XF4-2、XF4-5
XF2-4	SF2-1、XF2-3		
D3-3	D3-2	D4-1	XF4-1

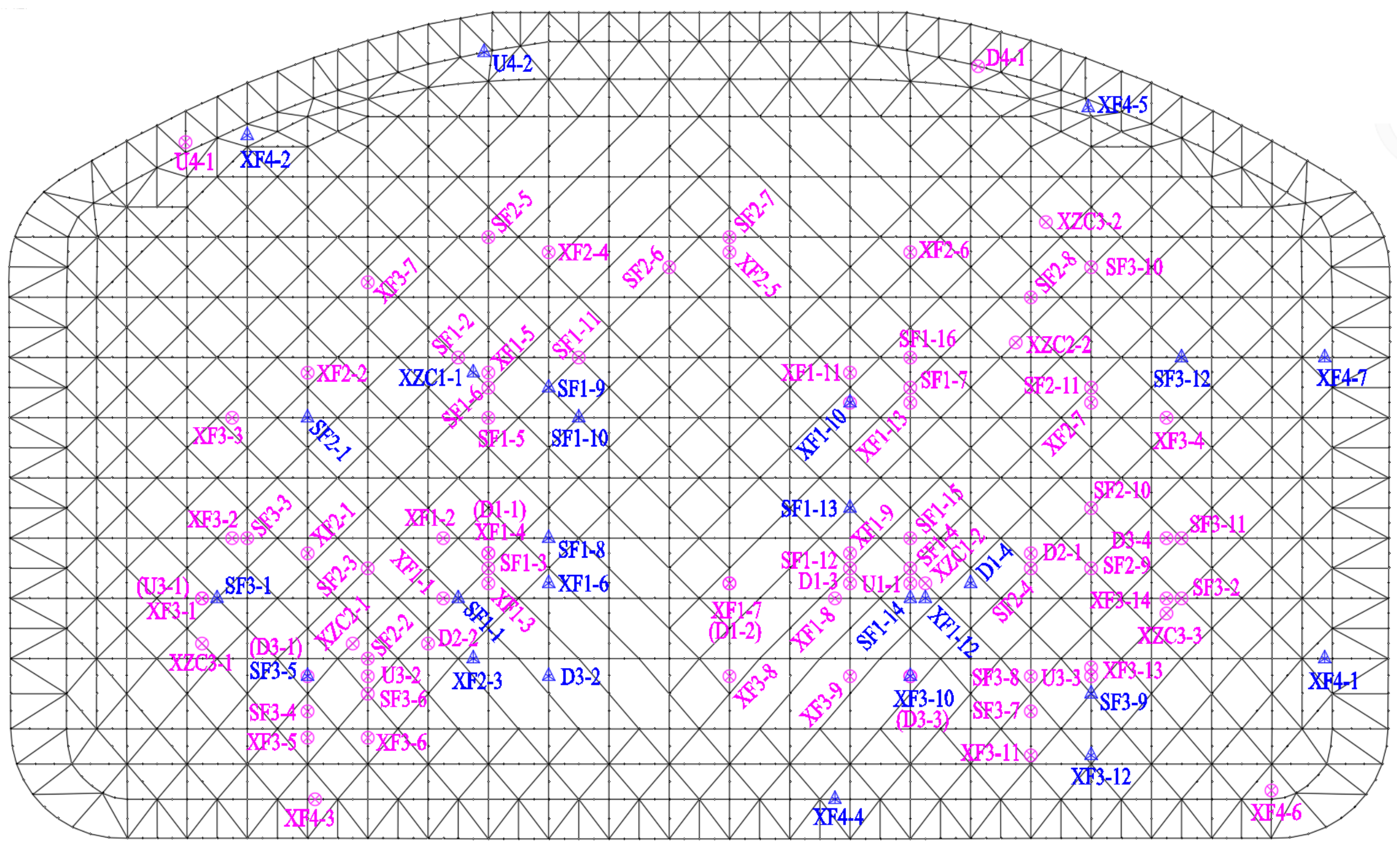

Note: “ ⊗ ”in the figure represents the test points determined after optimization
“ △ ” indicates the number of points that can be reduced after optimization

Fig. 6 Schematic diagram of optimal arrangement of measuring points

5. Response prediction based on LSTM neural network

In order to verify the reliability of the aforementioned optimization plan of measurement points, the response correlation between cross-correlated measurement points needs to be verified. The LSTM neural network technology, which is good at solving timing problems in deep learning, is used to establish a response prediction model. The on-site monitoring response values of the optimized measuring points are used to predict the response values of the measuring points that are eliminated during the optimization process but are cross-correlated with the optimized measuring points. At the same time, in addition to arranging sensors at optimized measuring points during the construction process, this paper also deliberately arranged sensors at cross-correlated measuring points, and compared the on-site monitoring data of these measuring point with its corresponding predicted values to verify the feasibility of optimization method of measuring points.

5.1. On-site monitoring

Since the bar of the space grid structure is mainly subjected to axial force, but the strain sensor is arranged in the actual construction. To facilitate intuitive interpretation, the measured strain values are converted into stress values in this paper. The strain sensor arranged in this paper has a measuring accuracy of 0.1%F. S and a resolution of 0.025%F. S, as shown in Fig.7. It is arranged in the middle position along the axis of the rod of its measuring point. The entire construction process is based on time series, with a total of 250 sets of data collected in the first construction stage, 500 sets of data in the second stage, 300 sets of data in the third stage, and 300 sets of data in the fourth stage. Due to the large amount of data, this paper does not list the detailed monitoring data due to space limitations.

Fig. 7 The strain sensor

5.2. LSTM neural network structure

Long short-term memory (LSTM) neural network is a special recurrent neural network suitable for processing and predicting time series problems[14-15]. As illustrated in Fig.8, the architecture consists of three control gates—the forget gate, input gate, and output gate—whose activation functions follow the classical LSTM design paradigm[16–18]. Specifically, the gating units employ the Sigmoid function (output range: 0 to 1), while the state units utilize the Tanh function (output range: -1 to 1). This configuration combines mathematical rigor with engineering advantages: the saturating nature of the Sigmoid function inherently aligns with gating logic, where 0 denotes complete information blocking and 1 indicates full transmission, while the zero-centered output and stronger gradient (maximum 1.0) of the Tanh function facilitate state updates and mitigate gradient vanishing in long-term dependency learning. Through these gating mechanisms, the LSTM achieves selective information transmission and state updating.

The forget gate regulates information flow from the previous cell state C_{t-1} to the current cell state C_t, with its output F_t calculated by the sigmoid function as shown in Formula (24) to represent the retention probability within the range of 0 to 1. The input gate controls the integration of new input X_t into the cell state C_t through a two-layer structure: the sigmoid layer (Formula (25)) generates an update factor I_t to realize weighted control over new inputs; the tanh layer generates candidate memory $\hat{C}_t$ (expressed by Formula (26)), whose output range of -1 to 1 can capture positive and negative features, and its stronger gradient property helps alleviate the gradient vanishing problem. The output gate regulates information output, with its output O_t calculated by the sigmoid function (Formula (27)), while the final hidden state H_t is obtained by scaling the cell state via the tanh function as shown in Formula (28), ensuring output range constraint and feature consistency.

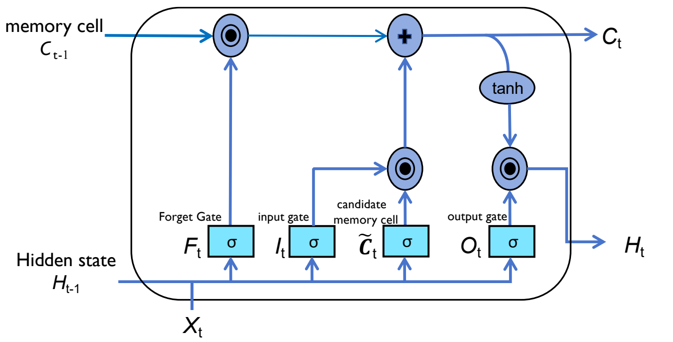

Fig. 8 Structural schematic diagram of LSTM

Note: σ in the figure represents the sigmoid function, and tanh represents the hyperbolic tangent function.

$$F_t = \sigma\left(W_f \cdot [H_{t-1}, X_t] + b_f\right) \tag{24}$$

$$I_t = \sigma\left(W_i \cdot [H_{t-1}, X_t] + b_i\right) \tag{25}$$

$$\hat{C}_t = \tanh\left(W_c \cdot [H_{t-1}, X_t] + b_c\right) \tag{26}$$

$$O_t = \sigma\left(W_o \cdot [H_{t-1}, X_t] + b_o\right) \tag{27}$$

in the above formula, W represents the network weight matrix, and b represents the network bias vector.

$$H_t = O_t \cdot \tanh\left(C_t\right) \tag{28}$$

The cell state C_t is continuously updated from the C_{t-1} of the previous moment according to the above process, and its update process is shown in formula (29).

$$C_t = F_t \cdot C_{t-1} + I_t \cdot C_t \tag{29}$$

When using the LSTM neural network to establish a correlated prediction model between measurement points for the central roof steel structure of Mall of China, the input data should be prepared first. In order to ensure the training effect, the input data should be sufficient. The principle of prediction is mainly to selectively memorize or forget training data, write down important information, and forget information of little value. By learning important information, long-term memory can be formed, which can then play a predictive role[19].

The actually arranged measuring points on the structure and their corresponding cross-correlated measuring points have a strong correlation in each construction stage. However, considering that the correlation rules in different construction stages may change significantly, each construction stage is analyzed separately. For illustrative purposes, the prediction process of the LSTM neural network is demonstrated using the cross-correlation monitoring points D1-1/SF1-8 and U4-1/XF4-4 as examples. Here, D1-1/SF1-8 belongs to the promoted zones I and II, encompassing four construction stages with 250, 500, 300, and 300 data samples collected in stages 1 to 4, respectively; U4-1/XF4-4 is located in the bulk material zone, comprising two construction stages with 500 and 350 data samples in stages 1 and 2, respectively. During training, the monitoring response data from points D1-1 and U4-1 are used as model inputs, while the corresponding response data from points SF1-8 and XF4-4 serve as outputs, thereby establishing a response prediction model between the respective monitoring points. The monitoring data at each stage are used as model data sets for training. For each stage, 1/5 of the data is used as the test set. The selection principle of test set is t=5d (d=1, 2, 3, ...), that is, every fifth group of data is taken as the test set, and the remaining data as the training set.

It is worth mentioning that regularization can make the gradient of the optimization loss function more stable to a certain extent, thereby improving the training speed and accuracy of the model[20], at the same time, regularization can also make the data in the model tend to be unified in the end, which is convenient for evaluation. Therefore, the maximum and minimum regularization method is used to standardize all data during the training process, and the processing process is shown in formula (30).

$$x' = \frac{x - x_{\min}}{x_{\max} - x_{\min}} \tag{30}$$

In the formula, x is the monitoring response data of the measuring point; x_{min} is the minimum value in the monitoring response data group of the measuring point; x_{max} is the maximum value in the monitoring response data group of the measuring point.

In addition, during the training process of LSTM model, parameters such as the number of network layers, the number of hidden layer units, the batch size, the maximum number of iterations, the learning rate, the loss function and the optimizer in the model all directly affect its training effect, so there is a necessity for set and optimization. In particular, the choice of loss function and optimizer is crucial to the normal operation of the model, because the loss function is used to measure the difference between the model's predicted output value and the true value. The essence of the LSTM training process is to minimize the loss function. At present, common loss functions include mean square error function (MSE) and cross entropy function (CE). MSE is often used in regression tasks, and CE is often used in classification tasks. This paper chooses the loss function of MSE, as shown in formula (31). In terms of selecting an optimizer, the gradient descent algorithm of adaptive moment estimation (Adam) is currently the most commonly used. This algorithm has the advantages of fast convergence speed, small memory usage, and better learning effect. Therefore, this paper chooses the Adam algorithm to optimize the training of the model.

$$\mathrm{MSE} = \frac{1}{n}\sum_{t=1}^{n}(x_t - \hat{x}_t)^2 \tag{31}$$

In the formula, n is the number of samples; x_t is the actual monitoring value; and $\hat{x}_t$ is the predicted model value.

In terms of model performance evaluation, the root means square error (RMSE) and the mean absolute error (MAE) can usually be selected to evaluate the model prediction accuracy, and their calculations are shown in formulas (32) and (33) respectively. Among them, RMSE can reflect the degree of dispersion between the predicted model value and the real value; MAE can reflect the closeness between the predicted model value and the real value. The smaller the value of each indicator is, the smaller the error between the predicted model value and the real value is, and the better the training effect is.

$$\mathrm{RMSE} = \sqrt{\frac{1}{n}\sum_{t=1}^{n}(x_t - \hat{x}_t)^2} \tag{32}$$

$$\mathrm{MAE} = \frac{1}{n}\sum_{t=1}^{n}|x_t - \hat{x}_t| \tag{33}$$

During the specific training process, the LSTM neural network prediction model was constructed using Matlab software (its architecture shown in Fig.9), which takes input features and processes them sequentially through an LSTM layer to capture temporal dependencies, followed by a Dropout layer to randomly discard neurons and suppress overfitting, then another LSTM layer to further refine feature learning, another Dropout layer to further enhance generalization, and finally a fully connected layer to integrate features and generate output for effective sequence data processing and feature extraction.

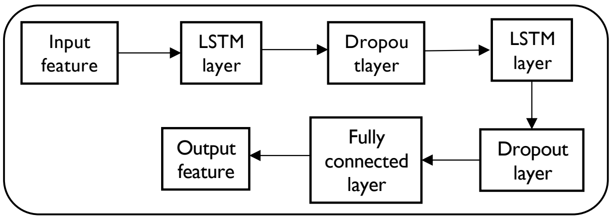

Fig. 9 Structural of the LSTM prediction model

The grid search method[21] was employed to iteratively optimize the number of network layers, hidden layer units, maximum iterations, and learning rate, with key parameters selected as shown in Table 4. The optimal values were selected based on the MSE from 5-fold cross-validation, where validation subsets were exclusively partitioned from the training set. A 2-layer LSTM architecture was adopted, reducing cross-validation MSE by 12.7% compared to a single layer and enhancing complex pattern fitting. The unit configuration (15,5) yielded a stable plateau in cross-validation MSE during later training stages (fluctuation range < ±0.003), effectively balancing model accuracy with computational efficiency. Dropout layers (rate = 0.2) were applied after each LSTM layer for regularization[22], achieving minimal cross-validation MSE fluctuation (±0.003) and optimal overfitting suppression. A learning rate of 0.001 ensured stable gradient updates and a cross-validation MSE of 0.080; higher rates (⩾0.01) caused gradient oscillation, while lower rates (0.0001) hindered convergence. Given the moderate training sample size, full-batch training was employed. Final hyperparameter evaluation on an independent test set confirmed generalization stability, with test MSE consistent with cross-validation trends.

Model convergence exhibits three distinct phases—rapid learning, stable convergence, and saturation plateau. As shown in Fig.10, epochs 0–500 involve rapid fitting of basic temporal features, with RMSE and loss decreasing sharply; epochs 500–3000 see the model capturing core patterns, slowing RMSE decline as it enters the diminishing returns zone; and epochs 3000–4000 maintain RMSE below 0.1 with minimal fluctuation, indicating convergence saturation. Further training risks overfitting, wastes computational resources, and yields no accuracy gains, thus the optimal maximum training iterations are set to 4000.

Table 4
Hyperparameter Search Space

Types of hyperparameters	Search range	Optimal value
Number of LSTM layers	{1, 2}	2
Cell array combination	{(10), (15), (20), (10,5), (15,5)}	(15, 5)
Dropout rate	{0.1, 0.2, 0.3, 0.4}	0.2
Learning rate	{0.1, 0.01, 0.001, 0.0001}	0.001
Maximum number of iterations	{3000, 4000, 5000}	4000

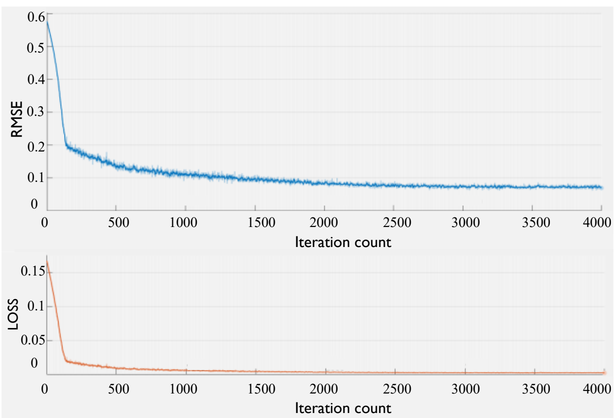

Fig. 10 The RMSE curve and loss curve during the training process

5.3. Prediction result analysis

The trained model was employed to predict the data of the test set, and the model evaluation indicators for members SF1-8 and XF4-4 at each construction stage were calculated according to Equations (32) and (33), as presented in Tables 5 and 6. The results indicate that the error metrics of the model at each stage are relatively small, demonstrating that the prediction accuracy falls within an acceptable range. To more intuitively illustrate the predictive performance of the model, a visual comparative analysis of the trends between the predicted and actual values at each stage was conducted, as shown in Fig.11 and Fig.12.

Table 5
Measurement point SF1-8 prediction error table

Construction phase	RMSE	MAE	Absolute maximum error (MPa)
Stage 1	2.7391	2.1410	9.32
Stage 2	2.2475	1.8384	6.33
Stage 3	0.8145	0.6967	1.651
Stage 4	3.2557	2.7640	6.58

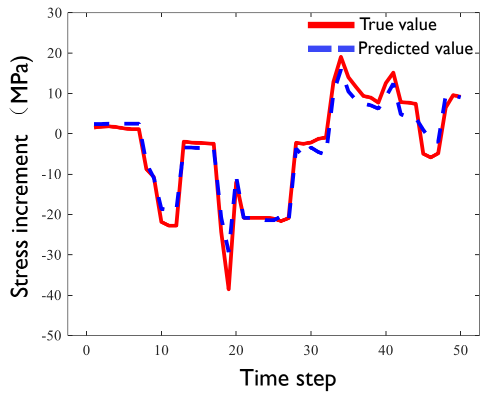

(a)The first stage

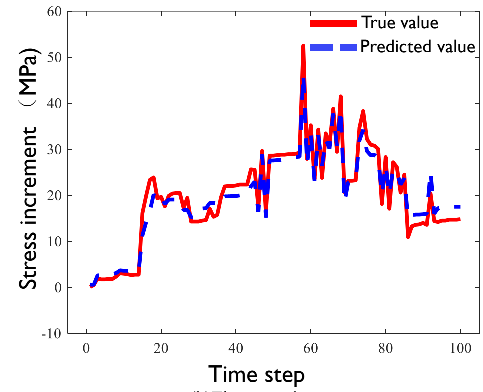

(b)The second stage

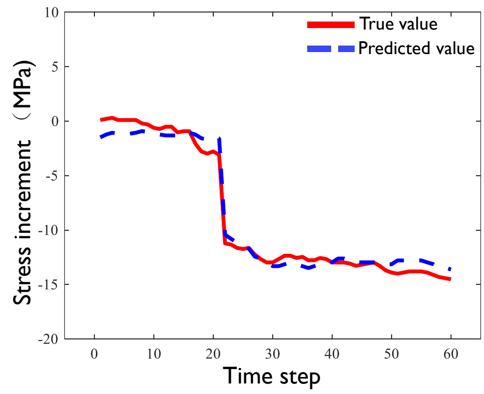

(c)The third stage

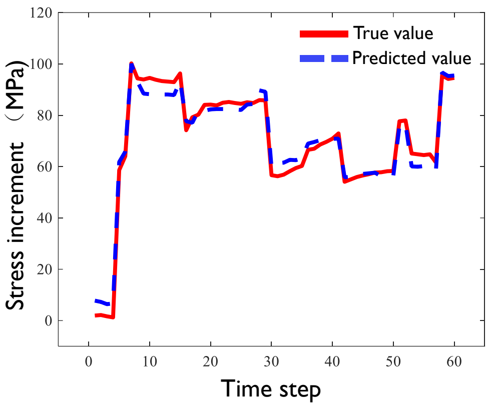

(d)Fourth stage

Fig. 11 SF1-8 Prediction via LSTM model

Table 6
Measurement point XF4-4 prediction error table

Construction phase	RMSE	MAE	Absolute maximum error (MPa)
Stage 1	1.4382	1.1142	3.36
Stage 2	2.2403	1.0917	2.15

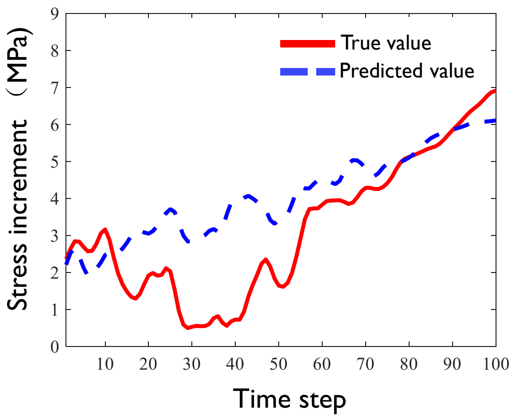

(a)The first stage

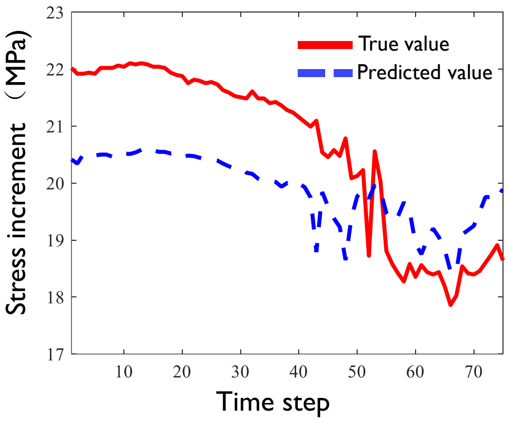

(b) The second stage

Fig. 12 XF4-4 Prediction via LSTM model

As shown in Fig.11, the Pearson correlation coefficient and Type-B grey relational degree effectively reveal the similarity in magnitude and trend of structural response variations. The model predictions closely follow the actual trends across construction stages, accurately capturing stress variations at SF1-8 despite fluctuations, thereby demonstrating the LSTM model's ability to learn the response correlation between optimized and cross-correlated measurement points. However, as shown in Fig.12, its prediction accuracy for the diagonal web member XF4-4 is lower than for SF1-8, due to XF4-4's more complex loading conditions, including combined vertical and horizontal forces, greater sensitivity to structural deformation, and additional joint moments, leading to a more intricate stress response.

The effectiveness of the LSTM model stems from its ability to capture the dynamic evolution of response correlations among key measurement points across construction stages, reflecting the combined influence of structural system transformations, load path redistributions, and construction sequence dependencies. In Stage 1, falsework unloading in Zone II shifts the load-bearing mode from falsework support to Zone I lifting points, reducing system stiffness and weakening measurement point correlations. Stage 2 integrates Zone III into a spatial grid, significantly increasing stiffness and enhancing correlations, demonstrating the transition from discrete components to global coordination. The construction sequence critically affects load path continuity—sequential lifting (Zone I then Zone II) reduces Stage 1 correlations, while synchronous lifting mitigates this effect. Stage 3's support removal redirects load paths, causing a sharp correlation drop, while the "central-to-peripheral" Zone III installation promotes stepwise stiffness growth. By Stage 4, the self-supporting system stabilizes, fixing load distribution and correlations.

Multi-stage analysis overcomes single-stage limitations by tracking correlation network evolution: (1) detecting transient events (e.g., Stage 3's unloading-induced correlation mutations); (2) quantifying construction sequence impacts on stiffness accumulation; and (3) enabling the LSTM model to learn time-varying behaviors via stage encoding, improving prediction generalization.

5.4. Applicability verification of prediction model under accidental load

During the construction process, the structure may bear a large concentrated load in a local area because of some unexpected situations, resulting in the sudden increase of stress of some members. In order to test whether the LSTM prediction model can accurately predict the sudden accidental action response, the SF1-8 in the upgrading process of zone 1 is taken as an example to verify it.

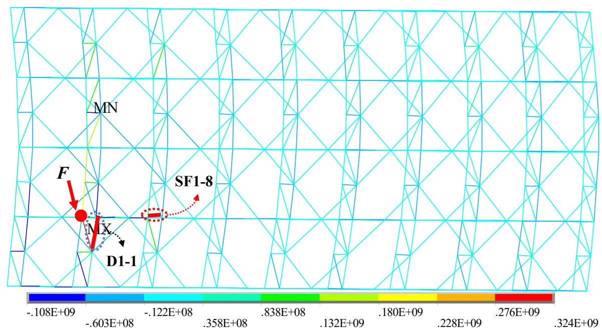

Fig. 13 Stress distribution diagram

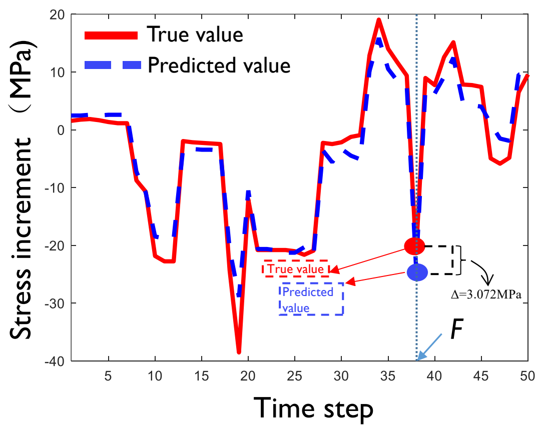

Fig. 14 Prediction of member SF1-8 during first stage

It is assumed that a vertical concentrated load F=-250kN is suddenly applied to the node as shown in Fig.13 during the lifting process of zone 1. The finite element calculation shows that under the action of F, the stress of D1-1 will change from -18.43MPa to -42.708MPa, and the stress increment is -24.665MPa; while the stress of SF1-8 will change from -11.774MPa to -33.132MPa, and the increment is -21.358MPa. In actual project, a sensor is arranged on D1-1, so we input the stress increment value of D1-1, namely, -24.665MPa into the LSTM prediction model to obtain the stress variation trend of SF1-8, as shown in Fig.14. Specifically, the predicted stress increment value is -24.43MPa at the moment F is applied. Compared with the calculated value of SF1-8, the difference is only 3.072MPa. It can be seen that LSTM also maintains a good robustness to the sudden state in the construction process.

This section focuses on validating the core capability of the proposed LSTM-based model for predicting inter-point response correlations, demonstrating its satisfactory predictive performance under a single static load condition. The model's generalizability to complex loading scenarios—characterized by dynamic time-varying properties, variable load positions, and multi-directional force coupling—remains to be verified in future research.

6. Conclusions

Based on the characteristics of certain correlation between the responses of long-span spatial structures, this paper proposes a optimization method of multi-stage construction monitoring measurement points that considers the correlation of structural responses, and uses LSTM neural network to establish a structural response prediction model. The main conclusions are as follows:

(1) Pearson correlation coefficient and B-type gray correlation can effectively explore the similarity in change size and change trend between structural responses. The structural response comprehensive correlation matrix established based on this can quantify the correlation strength of the response of measuring points at different construction stages. Moreover, it is found that the response correlation rules of relevant measuring points in different construction stages are different.

(2) The clustering correlation matrix transformed by the bond energy algorithm can quickly realize the classification and optimization of measurement points for large-span spatial structures considering multiple construction stages. Compared with the traditional layout plan of construction monitoring measurement points, the optimization method of measurement points that considers the comprehensive correlation of responses can optimize the number of measurement points by up to 25%.

(3) The LSTM neural network can well learn the response correlation between each optimized measurement point and its corresponding related measurement point, and the prediction results have good accuracy.

Funding

National Natural Science Foundation of China (51708067); 2022 Technology Innovation and Application Development Project of Nanan District, Chongqing (2022).

Reference

[1] Jiaxin Peng. Response estimation method of spatial steel structures based on correlation analysis. Thesis, Harbin Institute of Technology, China,2019.

[2] Lu W, Wen R, Teng J, et al. Data correlation analysis for optimal sensor placement using a bond energy algorithm. Measurement 2016; 91: 509-518.

[3] Liming Zhu, Yilian Chen, Si Yubian, Et al. Multi-sensor correlation analysis of bridge strain monitoring. China: MCC Building Research Institute Limited. Proceedings of the Industrial Architecture Symposium 2020 (Part 2).

[4] Beygzadeh S, Salajegheh E, Torkzadeh P, et al. An Improved Genetic Algorithm for Optimal Sensor Placement in Space Structures Damage Detection. International Journal of Space Structures. 2014; 29(3):121-136.

[5] Hui Feng. Local response correlation modeling method for Bridges based on recurrent neural networks. Thesis, Harbin Institute of Technology, China, 2019.

[6] Kaveh A, Dehkordi MR. Neural Networks for the Analysis and Design of Domes. International Journal of Space Structures. 2003;18(3):181-193.

[7] Jianxi Yang, Likai Zhang, Ren Li, et al. Damage identification of bridge structures using convolutional and long and short memory neural networks. Journal of Railway Science and Engineering 2020; 17(08): 1893-1902.

[8] Li Chao. Optimization and reconstruction of multi-type monitoring information based on correlation. Thesis, Harbin Institute of Technology, China, 2015.

[9] AlMahmoud H R, Hammo B, Faris H. A modified bond energy algorithm with fuzzy merging and its application to Arabic text document clustering. Expert Systems With Applications 2020; 159:1-24.

[10] ZHU Yinjuan, LI Haibo, et al. Method of resource combination based on relevance degree in cloud manufacturing environment. Computer Engineering and Applications 2016; 52(5): 255-261.

[11] Rahimi H, Parand F A, Riahi D. Hierarchical simultaneous vertical fragmentation and allocation using modified Bond Energy Algorithm in distributed databases. Applied computing and informatics 2018; 14(2): 127-133.

[12] Jialin Dong. Research on optimal arrangement of cable force sensors based on spatial correlation and inversion prediction of whole bridge cable force. Thesis, Harbin Institute of Technology, China, 2017.

[13] Runfa Wen. Research on structure monitoring method based on measurement point correlation analysis. Thesis, Harbin Institute of Technology, China, 2014.

[14] Jiayue X, Ge O. Predicting wind-induced structural response with LSTM in transmission tower-line system. SMART STRUCTURES AND SYSTEMS 2021; 28(3):391-405.

[15] Ye Z, Wen Z, Yanlong L, et al. A deep learning prediction model of DenseNet-LSTM for concrete gravity dam deformation based on feature selection. Engineering Structures 2023; 295:1-16.

[16] Hochreiter, S., & Schmidhuber, J. (1997). Long short-term memory. Neural computation, 9(8), 1735-1780.

[17] Gers, F. A., Schmidhuber, J., & Cummins, F. (2000). Learning to forget: Continual prediction with LSTM. Neural computation, 12(10), 2451-2471.

[18] Goodfellow, I., Bengio, Y., Courville, A., & Bengio, Y. (2016). Deep learning (Vol. 1, No. 2). Cambridge: MIT press.

[19] Hongtao Cui, Xiaoxu Chen, Chao Yang, etc. Subway inbound passenger flow prediction based on deep long short term memory network. Urban rail transit research 2019; 22(09): 41-45.

[20] Santurkar S, Tsipras D, Ilyas A, et al. How Does Batch Normalization Help Optimization. Canada: neural information processing systems, 2018.

[21] Yang Xiong, Shuqing Li, Hao Xu, et al. Research on short-term forecasting method of urban rail transit passenger flow. Electronic design engineering 2022; 30(01): 46-50.

[22] Xinyong Z, Liwei S, Lingtong Q. Bayesian Regularization Algorithm Based Recurrent Neural Network Method and NSGA-II for the Optimal Design of the Reflector. Machines 2022; 10(1) : 1-15.